AMPK- and cGAS-Mediated Dual Sensing of Glucose and dsDNA Synergizes to Enhance Antitumor Immunity

Ruyuan Zhou[1,2,3,#], Jingyan Pei[1,3,#], Shasha Chen[4], Qin Shen[1,3], Qirou Wu[3,5], Shengduo Liu[2,3], Chen Chen[1,3], Xin-Hua Feng[3,6], Jian Zou[7], Tingbo Liang[1,6], Y. Jessie Zhang[8], Sheng-Cai Lin[9], Penghong Song[1,*], Chen-Song Zhang[8,*], Qian Zhang[3,8,*], and Pinglong Xu[1,2,3,6,*]

[1] Department of Hepatobiliary and Pancreatic Surgery and Zhejiang Provincial Key Laboratory of Pancreatic Disease, The First Affiliated Hospital, School of Medicine, Zhejiang University, Hangzhou, 310058, China;

[2] Institute of Intellectual Medicine, ZJU-Hangzhou Global Scientific and Technological Innovation Center, Hangzhou, 310058, China;

[3] The MOE Key Laboratory of Biosystems Homeostasis & Protection and Zhejiang Provincial Key Laboratory of Cancer Molecular Cell Biology, Life Sciences Institute, Zhejiang University, Hangzhou, Zhejiang 310058, China;

[4] Zhejiang Provincial Key Laboratory for Water Environment and Marine Biological Resources Protection, College of Life and Environmental Science, Wenzhou University, Wenzhou 325035, China;

[5] Key Laboratory of Novel Targets and Drug Study for Neural Repair of Zhejiang Province, School of Medicine, Hangzhou City University, Hangzhou 310015, China

[6] Cancer Center, Zhejiang University, Hangzhou, Zhejiang 310058, China;

[7] Eye Center of the Second Affiliated Hospital School of Medicine, Institute of Genetics, School of Medicine, Zhejiang University, Hangzhou 310058, China;

[8] Department of Molecular Biosciences, University of Texas at Austin, Austin, TX 78712, USA;

[9] State Key Laboratory for Cellular Stress Biology, School of Life Sciences, Xiamen University, Xiamen, 361102, China;

[#] These authors contributed equally;

[*] Correspondence should be addressed to P.S., C.-S. Z., Q.Z., or P.X.

Address for correspondence:

Penghong Song

Department of Hepatobiliary and Pancreatic Surgery, The First Affiliated Hospital, School of Medicine, Zhejiang University

79 Qingchun Road, Hangzhou 310003, China

E-mail: songpenghong@zju.edu.cn

Chen-Song Zhang

State Key Laboratory for Cellular Stress Biology, School of Life Sciences, Xiamen University, Xiamen, Fujian, China

E-mail: cszhang@xmu.edu.cn

Qian Zhang

Department of Molecular Biosciences, University of Texas at Austin

100 E. 24th Street, Norman Hackerman Building (NHB) 4.130, Austin, TX 78712, USA

Tel: 1-512-471-1029

E-mail: qian.zhang1@austin.utexas.edu

Pinglong Xu

Life Sciences Institute, Zhejiang University

866 Yuhangtang Road, Nano Building, Room A555, Hangzhou, 310058, China

Tel: 86-571-88206078

E-mail: xupl@zju.edu.cn

Running Title: AMPK-TBK1 Integrates Glucose Availability to Antitumor Immunity

ABSTRACT

Intratumoral glucose availability is linked considerably to tumor growth, immune evasion, and metastasis. However, the precise molecular mechanisms by which glucose levels govern cellular and immune responses against tumors remain incompletely understood. Here, we explored the context of tumors of intersections between AMP-activated protein kinase (AMPK) and cGAS-STING signaling, a key pathway initiating antitumor immunity. We unexpectedly found that AMPK activation robustly enhances cGAS-STING signaling within cancer and immune cells, which potently impacts melanoma and colorectal cell senescence, organoid apoptosis, and the infiltration of $CD4^+$ and $CD8^+$ T lymphocytes. Using classic or newly developed AMPK agonist Aldometanib, $TBK1^{S511E/S511E}$ knock-in (KI) mice, glucose metabolic modulator, as well as AMPKα1/α2 dKO melanoma, we demonstrated that dual sensing of intratumoral glucose and dsDNA integrated by the AMPK-TBK1 cascade is essential for initiating antitumor immunity and suppressing cancer progressions. Notably, novel AMPK agonists or intervening in glucose glycolysis by Lonidamine synergized effectively with STING agonists, substantially inhibiting melanoma growth. Therefore, these findings unravel a concise mechanism integrating glucose metabolism and innate DNA sensing into cancer cell fate and propose an effective therapeutic strategy to enhance antitumor immunity.

Key Words: AMPK; TBK1; cGAS-STING; antitumor immunity; glucose metabolism; synergistic therapy; glucose sensing; nucleic acid sensing; AMPK agonists; senescence; apoptosis; dual sensing; T lymphocytes; melanoma; colorectal cancer; immunotherapy; immune evasion; glycolysis; tumor microenvironment; cancer immunology

78 **HIGHLIGHTS**

79 1. Dual and synergistic sensing of glucose and dsDNA facilitates antitumor immunity in
80 melanoma and colorectal cancer;
81 2. AMPK substitutes intratumoral cGAS-STING-IRF3 signaling through TBK1
82 phosphorylation at S511;
83 3. Glucose deficiency induces cancer cell senescence, apoptosis, and T lymphocyte
84 infiltration via the AMPK-TBK1 cascade;
85 4. Newly developed AMPK agonists synergize with STING agonists to retrieve striking
86 tumor suppression.
87
88

INTRODUCTION

Nucleic acid sensing surveils tissue abnormalities and pathogen invasion and establishes an immune state to restrict microbial infection, modulate adaptive immunity, and guide tissue repair and regeneration (Chan & Gack, 2015, Chen, Sun et al., 2016b, Roers, Hiller et al., 2016, Takeuchi & Akira, 2010, Zhang, Liu et al., 2022b). Pattern recognition receptors (PRRs) such as cGAS (Gao, Ascano et al., 2013, Sun, Wu et al., 2013) monitor microbes and tissue damage by perceiving cytosolic dsDNA derived from pathogens, the mitochondria, or the nucleus (Chen et al., 2016b, Hu & Shu, 2020, Roers et al., 2016, Takeuchi & Akira, 2010). Upon recognition of free dsDNA, cGAS synthesizes 2'3'-cyclic GMP-AMP (cGAMP)(Ablasser, Goldeck et al., 2013, Gao et al., 2013, Wu, Sun et al., 2013, Zhang, Shi et al., 2013), activates STING (also known as MITA or ERIS) (Ishikawa & Barber, 2008, Sun, Li et al., 2009, Zhong, Yang et al., 2008), which triggers the non-canonical STING-PERK pathway in the endoplasmic reticulum (ER) that regulates mRNA translation (Zhang et al., 2022b), induces non-canonical autophagy in the ERGIC (Gui, Yang et al., 2019), and facilitates the activation of TBK1 and IRF3 at the Golgi apparatus (Liu, Cai et al., 2015, Zhang, Shang et al., 2019). Phosphorylated IRF3 translocates into nuclear and transcribes type I interferons (IFN-Is) and numerous IFN-stimulated genes (ISGs) (Fitzgerald, McWhirter et al., 2003, Sharma, tenOever et al., 2003), in coordination with simultaneously activated NF-κB (Chen et al., 2016b, Roers et al., 2016, Takeuchi & Akira, 2010). Therefore, nucleic acid sensing induces mRNA translation arrest (Zhang et al., 2022b), autophagy (Gui et al., 2019, Pilli, Arko-Mensah et al., 2012, Wild, Farhan et al., 2011), phase separation (Meng, Yu et al., 2021), mitochondrial dynamics (Chen, Liu et al., 2020), cell differentiation (Xu, Bailey-Bucktrout et al., 2014), and triggers cell senescence (Dou, Ghosh et al., 2017, Gluck, Guey et al., 2017, Mackenzie, Carroll et al., 2017, Yang, Wang et al., 2017) and cell death (Cerboni, Jeremiah et al., 2017, Melki, Rose et al., 2017, Petrasek, Iracheta-Vellve et al., 2013).

Effects of cGAS-STING signaling in tumor biology are complex and multifaceted (Samson & Ablasser, 2022). cGAS-STING signaling is active in cancerous, immune, and stromal cells, shifting their cellular function, metabolism, and fate. The activation of cGAS-STING signaling releases various IFN-I, cytokines, cGAMP, and DNA, which attracts and matures dendritic cells, macrophages, natural killer cells (NKs), and effector T lymphocytes to mount an

antitumor immunity (Chin, Sulpizio et al., 2022, Kwon & Bakhoum, 2020). STING-induced senescence and immune microenvironment modulation also participate in antitumor immunity regulation, positively or negatively [(Chen & Xu, 2023),(Bakhoum, Ngo et al., 2018),(Chen, Boire et al., 2016a),(Hong, Schubert et al., 2022),(Li, Mirlekar et al., 2022),(Concepcion, Wagner et al., 2022)], and STING-dependent residency of tumor-associated macrophages (TAMs) attenuate its antitumor role (Zhou, Wang et al., 2024). Therefore, the effects of cGAS-STING in cancer biology could be context- and stage-dependent and should be carefully evaluated during cancer treatments.

Cells in multicellular organisms depend on balanced nutrient availability for survival, growth, and defense. Despite this, the direct molecular connection between nutrient sensing and tissue damage perception remains less understood. AMP-activated protein kinase (AMPK) plays a central role in detecting glucose deficiency and controlling metabolic pathways (Hardie & Ashford, 2014, Hardie, Ross et al., 2012, Lin & Hardie, 2018). AMPK is activated at the lysosomal surface in response to low glucose levels through aldolase and the v-ATPase-Ragulator complex(Zhang, Hawley et al., 2017a, Zhang, Jiang et al., 2014, Zhang, Li et al., 2022a), in addition to being induced by AMP/ATP ratios and kinase such as LKB1 or CaMKII (Garcia & Shaw, 2017, Gonzalez, Hall et al., 2020, Hardie et al., 2012). AMPK masterly regulates an array of cellular processes such as glucose and lipid metabolism, protein synthesis, autophagy, mitochondrial biogenesis, and overall metabolism (Hardie et al., 2012, Mouchiroud, Eichner et al., 2014), and its dysfunction is broadly accompanied by obesity, type 2 diabetes, and cancers. We recently reported that viral infection causes a rapid and dramatic decrease in blood glucose levels and substantially activates AMPK in tissues, which directly phosphorylates TBK1 to trigger IRF3 recruitment and assemble MAVS or STING signalosomes, thus effectively mounting antiviral immunity(Zhang, Liu et al., 2022c). In adipocytes, TBK1 also represses energy expenditure by inhibiting AMPKα (Zhao, Wong et al., 2018). These observations indicate the presence of the intersection between metabolic master kinase AMPK and immune key kinase TBK1. Nevertheless, the roles of metabolism and immunity crosstalk through AMPK-TBK1 signaling in the context of malignant diseases remain poorly understood.

However, hyperglycemia has been considerably linked to diabetes-related vulnerability to malignancy (Klil-Drori, Azoulay et al., 2017), and it impacts cancer immunology in distinct

149 ways. For instance, elevated glucose levels through the hexosamine biosynthesis pathway
150 (HBP) enhance the O-GlcNAcylation level in TAMs, promoting M2-like polarization and
151 cancer progression (Rodrigues Mantuano, Stanczak et al., 2020). In diet-induced obesity,
152 more immunosuppressive myeloid-derived suppressor cells (MDSCs) were observed with
153 higher tumor progression of pancreatic cancer (Clements, Long et al., 2018, Incio, Liu et al.,
154 2016). Meanwhile, tumor cells typically exhibit increased glucose uptake and enhanced
155 glycolysis, which supports key processes for tumorigenesis, such as the biosynthesis of
156 nucleotides, amino acids, and lipids. Focusing on the AMPK-TBK1 axis, here we
157 systematically investigated the link between glucose availability and antitumor immunity.
158 Using the well-documented and newly developed AMPK agonists and TBK1 S511E knock-in
159 (KI) mice, we found that activated AMPK directly phosphorylated intratumoral TBK1 at S511,
160 promoting cGAS-STING-initiated senescence and antitumor immunity, thereby attenuates
161 the progression of melanoma and colorectal cancer. In summary, we proposed an
162 intratumoral dual and synergistic sensing of dsDNA and glucose, which forms a "metabolism
163 and immune sensing" bridge through the concise AMPK-TBK1 signaling and determines
164 tumor progression.
165

166 **RESULTS**

167 **Glucose deficiency promotes intratumoral cGAS-STING signaling**

168 To explore the function of glucose metabolism on antitumor immunity in TME, we
169 investigated the state of glucose deficiency and its impacts on cGAS-STING signaling, an
170 innate immune pathway crucial in antitumor immunity. Intratumoral glucose deficiency was
171 evident, as reported (Keerthana, Rayginia et al., 2023, Ramakrishnan, Terry et al., 2025,
172 Reinfeld, Madden et al., 2021), and as indicated by AMPK-induced phosphorylation of
173 metabolic regulator ACC1 in melanoma (Fig. 1A-1B). pACC1 signal was particularly robust at
174 tumor edges, where proliferating tumor cells and immune cells need high glucose demand.
175 cGAMP treatment in primary peritoneal macrophages (PMs) triggered robust activation of
176 TBK1 and IRF3, the central kinase and key signaling mediator of cGAS-STING signaling.
177 Simulating an intratumoral glucose-depleted microenvironment using 2-deoxy-D-glucose (2-
178 DG) resulted in an enhanced cGAS-STING-IRF3 pathway when compared to energy-sufficient
179 conditions, accompanied by robust activation of AMPK (Fig. 1C). We observed a similar
180 enhancement of cGAS-STING signaling in colorectal adenocarcinoma cells (DLD1) and mouse
181 embryonic fibroblasts (MEFs) under energy-deficient conditions (Figs. 1D-1E). AICAR, a well-
182 established AMPK agonist (Corton, Gillespie et al., 1995), expectedly facilitated cGAS-STING
183 signaling in fibroblasts and cancer cells (Figs. 1D-1E). Likewise, glucose depletion amplified
184 mitochondrial DNA (mtDNA)-induced activation of cGAS-STING-IRF3 signaling in colorectal
185 carcinoma cells (Fig. 1F), achieved by combinational treatment of ABT-737, qVD-OPH, and
186 S63845 (AQS) (McArthur, Whitehead et al., 2018, Rongvaux, Jackson et al., 2014, White,
187 McArthur et al., 2014). AICAR also potentiated the sensing of cytosolically exposed dsDNA in
188 DLD-1 cells, simulated by poly(dA:dT) transfection (TpdAdT) (Fig. 1G). These observations
189 across immune cells, fibroblasts, and cancer cells suggest that glucose deficiency, frequently
190 seen in tumors, significantly augments cGAS-STING signaling and is likely through AMPK
191 activation.

192

193 **AMPK facilitates cGAS-STING signaling in cancer cells by TBK1 S511 phosphorylation**

194 To validate that glucose deficiency regulates nucleic acid sensing through AMPK activation,
195 we generated AMPK α1/α2 dKO cells in B16-F10 melanoma cells using a CRISPR-mediated

196 approach (Fig. 2A). Genetic deletion of AMPK catalytic subunits α1/α2 attenuated cGAS-
197 STING-IRF3 signaling in B16 melanoma, as indicated by reduced levels of phospho-STING
198 (S366) and phospho-IRF3 (S396) (Fig. 2A). Likewise, deletion of AMPK α1 and α2 subunits in
199 colorectal carcinoma HCT116 cells similarly decreased RLR-MAVS-IRF3 signaling (Fig. 2B), the
200 dsRNA pathway with an emerged role in antitumor immunity (Chiappinelli, Strissel et al.,
201 2015, Sasaki, Homme et al., 2024). The role of AMPK on TBK1 activation was also evident as
202 AMPK catalytic subunits strongly potentiated the TBK1-IRF3 interaction (Fig. 2C) and TBK1-
203 stimulated IRF3 transactivation (Fig. 2D). Our previous study and the mass spectrometry
204 analyses of AMPK-coexpressed TBK1 have identified that the S511 residue on TBK1 is
205 abundantly modified by AMPKα1 (Zhang et al., 2022c). We found that AMPK inhibitor
206 dorsomorphin (Compound C) abolished TBK1 S511 phosphorylation (Fig. 2E), and an
207 antibody specifically recognizing phospho-TBK1 S511 demonstrated that AMPKα1 directly
208 phosphorylated TBK1 at this residue (Fig. 2F). We thus evaluated the capability of wild-type,
209 phospho-resistant (S511A), and phosphomimetic TBK1 (S511E) to activate IRF3 by an IRF3-
210 responsive reporter, which indicated that AMPK-mediated TBK1 phosphorylation at S511
211 was critical for driving IRF3 transactivation (Fig. 2G). Expectedly, a compromised interaction
212 between phospho-resistant TBK1 and IRF3 was seen (Fig. 2H). These findings suggest that
213 AMPK enhances cGAS-STING signaling by phosphorylating TBK1 at S511 to prime TBK1
214 activation.

215 To validate this AMPK-TBK1 axis in cancer cells, we generated and examined knock-in (KI)
216 clones of colorectal cells DLD1 with mutations that either prevent (S511A) or mimic (S511D)
217 AMPK-mediated modification by CRISPR-based genome editing (Zhang et al., 2022c). cGAS-
218 STING signaling was attenuated when endogenous TBK1 was mutated into the S511A variant
219 that resists AMPK modification (Fig. 2I). Conversely, STING signaling was robustly activated
220 when endogenous TBK1 was mutated to the S511D variant that mimics AMPK-TBK1
221 phosphorylation, to a level comparable to those under AICAR treatment (Fig. 2J). Noticeably,
222 the AICAR-enhanced activation of STING signaling was absent in these DLD1 KI cells (Fig. 2J).
223 These observations suggest that AMPK-mediated TBK1 phosphorylation at residue S511 is
224 critical for cancer cells to respond to glucose deficiency.
225

226 **AMPK drives STING-induced cancer cell senescence and apoptosis**

227 cGAS-STING responds to dsDNA leakage and drives cellular senescence, which could be
228 important in tumor growth arrest and potentially in antitumor immunity (Dou et al., 2017,
229 Gluck et al., 2017, Yang et al., 2017). We found that upon chemical induction of DNA damage,
230 colorectal carcinoma DLD1 cells displayed strong phenotypes of cellular senescence,
231 evidenced by SA-β-Gal staining and senescence-associated secretory phenotypes (SASPs)
232 (Fig. 3A-3B). Genetic ablation of AMPK α1/α2 subunits endowed DLD1 with apparent
233 resistance to DNA damage-induced cellular senescence (Fig. 3A). By contrast, AICAR
234 facilitated the progression of these colorectal cancer cells into senescence (Fig. 3B). In
235 agreement with these observations, simulating the glucose-depleted microenvironment
236 using 2-DG greatly enhanced DLD1 senescence (Fig. 3C). We further found that by utilizing a
237 zebrafish model of damage-induced senescence, AMPK activation by AICAR promoted
238 camptothecin (CPT)-induced senescence in zebrafish, indicated by increased numbers of SA-
239 β-Gal-positive cells in the heads and tails of zebrafish (Fig. 3D). Inhibition of AMPK by
240 dorsomorphin strongly attenuated CPT-induced senescence, as expected (Fig. 3D). These
241 observations suggest that AMPK is critical to regulate damage-induced cellular senescence,
242 mediated by cGAS-STING signaling.

243 The activation of cytosolic dsDNA sensing also mediates a context-dependent apoptotic
244 program (Gulen, Koch et al., 2017), an evolved strategy beneficial to tissue homeostasis and
245 immune modulation. We found that activation of cGAS-STING by DNA damage inducer HU
246 (Wu, Zhang et al., 2019) triggered significant levels of colorectal cancer cell apoptosis, which
247 was noticeably regulated by AICAR and dorsomorphin (Fig. 3E). Additionally, by utilizing *in*
248 *vitro*-cultured intestinal organoids, we detected a strong phenotype of HU-induced
249 apoptosis among intestinal cells, which was further exaggerated by AMPK activation (Fig. 3F).
250 These observations suggest that glucose deficiency and resulting AMPK activation controls
251 both senescence and apoptosis of cancer and functional cells through an AMPK-TBK1 axis.

252

253 **AMPK-TBK1 signaling facilitates STING-mediated antitumor immunity in melanomas**

254 Next, we utilized a naturally occurring and constitutively active STING SAVI mutant (R281Q)
255 to generate B16-F10 melanoma with inducible and constitutively active STING signaling.

256 Upon implanting subcutaneously into wild-type C57BL/6 mice, we found that melanomas
257 harboring STING R281Q SAVI mutation exhibited significantly reduced growth (Figs. 4A-4C),
258 attributed mainly from STING-induced expression of type I interferons (IFNs) (Wu et al.,
259 2019). Increased immune cells infiltrated these melanomas with constitutive STING signaling,
260 particularly T cells (Figs. 4D-4E), indicating enhanced antitumor immunity. Administration of
261 AMPK agonist AICAR significantly intensified T lymphocyte infiltration in melanomas (Figs.
262 4D-4E) and suppressed tumor growth substantially (Figs. 4A-4C), suggesting that AMPK can
263 amplify STING-mediated antitumor immunity in melanoma.

264 To determine whether the AMPK-TBK1 axis mediates this enhanced antitumor
265 immunity effects, we generated knock-in (KI) mice harboring the TBK1 S511E mutation using
266 a CRISPR-mediated strategy (Zhang et al., 2022c), which mimics AMPK-mediated TBK1
267 phosphorylation. The TBK1 S511E homozygous mice were viable, fertile, and appeared
268 phenotypically normal. However, melanoma growth was markedly attenuated in these TBK1
269 S511E mice (Figs. 4F-4H), along with a significantly increased level of T lymphocyte
270 infiltration (Figs. 4I-4J). More elevated antitumor immunity was not seen in TBK1 S511E
271 knock-in mice in the presence of cGAMP (Figs. 4F-4H), further suggesting the importance of
272 AMPK-TBK1 signaling in this process. These consistent observations propose the AMPK-TBK1
273 axis as a critical factor in facilitating STING-mediated antitumor immunity.

274

275 **AMPK agonists synergize well with cGAMP to promote antitumor immunity in melanomas**

276 To evaluate the potential for improving intratumoral antitumor immunity through this
277 AMPK-TBK1 axis, we employed in the in vivo model of melanoma a well-characterized AMPK
278 agonist AICAR [(Corton et al., 1995)] and a newly developed AMPK agonist Aldometanib [(Zhang et al.,
279 2022a)], which acts through distinct mechanisms. As expected, administration of cGAMP in
280 mice, a natural STING ligand, resulted in significant tumor growth suppression. AICAR (Figs.
281 5A-5C) and Aldometanib (Figs. 5D-F) markedly enhanced melanoma growth arrest,
282 synergizing well with cGAMP. These findings suggest that maneuvering AMPK activation can
283 effectively strengthen STING-induced antitumor immunity. Intriguingly, we observed that
284 Aldometanib also enhanced antitumor effects in mice bearing AMPK dKO B16-F10
285 melanomas (Figs. 5G-5I), suggesting an additional cancer cell-nonautonomous effect of

Aldometanib in melanoma.

Interrupting aerobic glycolysis potentiates antitumor immunity through the AMPK-TBK1 cascade

Next, we interrupted glucose metabolism by inhibiting aerobic glycolysis in cancer cells using Lonidamine, a classical hexokinase inhibitor (Floridi, Paggi et al., 1981), to evaluate the potential of glucose metabolism intervention in antitumor immunity. Lonidamine interferes with energy metabolism and induces AMPK activation (Roberts, Tan-Sah et al., 2014, Wu, Zhang et al., 2023, Zhang et al., 2017a). Notably, we found that combinational use of cGAMP and Lonidamine resulted in substantial tumor growth arrest (Figs. 6A-6C), along with significantly increased infiltration of intratumoral T lymphocytes in melanomas (Figs. 6D-6E). Furthermore, we found that Lonidamine promoted the robust activation of intratumoral cGAMP-induced cGAS-STING signaling in B16-F10 melanomas, evidenced clearly by increased levels of STING clustering, phosphorylated STING (pSTING S365), and phosphorylated TBK1 (pTBK1 S172) (Fig. 6F). These findings suggest that targeting glucose metabolism enhances STING-mediated immunity and can be a promising strategy in antitumor therapeutic, such as in melanomas.

DISCUSSION

Tumor cell metabolism depletes essential nutrients in the tumor microenvironment (TME), leading to significant glucose competition between cancer and immune cells. Meanwhile, the intervention of cGAS-STING signaling is a significant feature of cancers, mainly by genetic deletion of signaling components and suppression of signaling cascades, which attenuates its beneficial roles in antitumor immunity (Ghosh, Saha et al., 2021, Meng et al., 2021, Wu et al., 2019). However, the exact mechanisms for cGAS-STING activation and its contribution to cellular behaviors in cancer and immune cells, such as cell death, senescence, IFN secretion, and metabolic changes, need further interrogation. This study elucidated how the glucose sensor AMPK senses intratumoral glucose abundance and promotes antitumor immunity through direct phosphorylation and activation of TBK1, an essential kinase during innate immune responses. Given the complex energy metabolism in TME, understanding the AMPK-TBK1 axis opens new avenues for targeting glucose metabolism in both cancer and immune cells. Through activating cGAS-STING signaling and enhancing T-cell-mediated antitumor immunity, these findings provide significant therapeutic targets for drug development in cancer immunotherapy.

Cancer cells primarily rely on aerobic glycolysis for energy metabolism, through which glucose is converted into lactic acid. This metabolic shift exacerbates glucose deficiency stress within the tumor, leading to metabolic competition between tumor cells and immune cells. Notably, these metabolic changes in immune cells contribute to establishing an immunosuppressive microenvironment for accelerating tumor growth and immune evasion. While previous studies have extensively characterized the Warburg effect and its impact on tumor proliferation and immune suppression, this study focuses on how metabolic sensing mechanisms combined with nucleic acid sensing influence the immune landscape of the TME. The cGAS-STING pathway facilitates immune cell recruitment and inhibits tumor progression through cellular senescence and apoptosis (Chen & Xu, 2023). A recent study has highlighted that the AMPK-TBK1 axis plays a crucial role in innate antiviral immunity, extending AMPK's function beyond its classical roles in glucose and lipid metabolism, protein synthesis, autophagy, and mitochondrial function (Zhang et al., 2022c). Changes in glucose metabolism in the TME are closely linked to immune responses. We found that the

interaction between AMPK and cGAS-STING forms a "metabolic and immune sensing" bridge, which synergistically senses the metabolic state of tumor cells and tumor microenvironment to decide the magnitude of immune responses during tumorigenesis. AMPK directly phosphorylates S511 residue on TBK1, enhancing STING-IRF3 signaling activation and promoting T-cell infiltration into the TME, significantly inhibiting melanoma growth. Therefore, these findings expand the understanding of metabolic integration in innate immunity and provide new insights into antitumor immunity.

New therapeutics for tumor treatment increasingly focus on regulating cellular metabolism and immune responses. We propose that modulating glucose levels within tumors, the activation state of AMPK, and the modulation of AMPK-TBK1 signaling could offer novel aspects for antitumor therapeutics. As a critical energy sensor, AMPK is activated in response to glucose deprivation, thereby adjusting the cellular metabolic state. Our study revealed that AMPK activation leads to direct phosphorylation of TBK1 at S511, enhancing cGAS-STING-IRF3 signaling and promoting antitumor immune responses and STING-induced cellular senescence and apoptosis, thereby potently inhibiting tumor growth. Besides, AMPK plays an important role in the adaptive stress response of tumor cells, regulating key metabolic pathways to inhibit tumor cell proliferation (Lin & Hardie, 2018). We supposed AMPK also influences the metabolism of immune cells in the TME, particularly macrophage polarization, which impacts tumor immune evasion. By modulating AMPK activity, immune cell surveillance of tumors can be enhanced through cGAS-STING signaling, effectively preventing tumor immune escape.

In conclusion, our study reveals the key role of the concise AMPK-TBK1 axis in regulating intratumoral glucose metabolism and promoting antitumor immune responses, which considerably connects glucose metabolism with innate immunity. We propose that targeting the AMPK-TBK1 axis, the intersection between intratumoral glucose metabolism and antitumor immunity, could reach a substantial synergy for cancer treatments.

ACKNOWLEDGMENTS

This research was sponsored by the NSFC Projects (32321002, 32430028, and 31830052 to P.X., 82271768 to Q.Z., and 82001668, 32370759 to S.C.) and the National Key Research and Development Program of China (2021YFA1301401 to P.X. and 2021YFD1801103 to Q.Z.). Thanks also to technical assistance by the Life Sciences Institute core facilities, Zhejiang University.

AUTHOR CONTRIBUTIONS

Q.Z. and R.Z. carried out most experiments. C.-S.Z., J.P., S.C., Q.S., Q.W., S.L., and C.C. contributed to several experiments. X.-H.F., J.Z., T.L., Y.J.Z., S.-C.L., P.S., and C.-S.Z. helped with reagents, data analyses, and discussions. P.X., Q.Z., and R.Z. conceived the study and experimental design and wrote the manuscript.

COMPETING FINANCIAL INTERESTS

The authors declare no competing financial interests.

MATERIALS AND METHODS

Mice

TBK1 S511E transgenic mice were on C57BL/6 background, and both male and female littermates were used in all the experiments. GemPharmatech generated TBK1 Knock-in transgenic C57BL/6 mice. To create point mutations (S511E) at mouse Tbk1 locus by CRISPR/Cas9-mediated genome engineering, Tbk1 S511E (TCT to GAA) specific sgRNA oligos were designed by the CRISPR website (http://crispr.mit.edu/) targeting sequence at S511 locus (5'- TTCTATTGTTCCCTGAGAAC -3') and (5'- ATTTAGCTTTCCAGTTCTCA -3'), with S511E oligo donor sequence (5'-CATTTGGATCTGATCCGTTGTTCTGACCTAACCTAACCCGTTGTATTTAGCTTTCCAGCGAACAGGGAAC AATAGAAAGCAGTCTTCAGGACATCAGCAGCAGGCTGTCTCCAGGGGGCT -3'). Cas9 mRNA and sgRNA generated by in vitro transcription and donor oligo were co-injected into fertilized eggs for knock-in mouse production. The target region of the mouse Tbk1 locus was sequenced to confirm targeting. All the animals were bred and maintained in a pathogen-free animal facility at the laboratory animal center of Zhejiang University. The care of experimental animals was approved by the Zhejiang University committee and followed Zhejiang University guidelines.

Zebrafish

Zebrafish AB wild-type embryos (male/female) were raised at 28.5°C in E3 egg water. The care of experimental animals was approved by the Zhejiang University committee and followed Zhejiang University guidelines.

Peritoneal Macrophages

Peritoneal macrophages were isolated from C57BL/6 mice at 6-8 weeks of age with the Brewer thioglycollate medium (Sigma-Aldrich)-induced approach. Three days after the intraperitoneal injection of 2.5 mL of 3% thioglycollate medium, peritoneal macrophages were isolated and cultured in the RPMI 1640 medium.

Cell Lines

HEK293, HCT116, DLD1, MEFs, and B16-F10 cells were from ATCC. No cell lines used in this

406 study were found in the database of commonly misidentified cell lines maintained by ICLAC
407 and NCBI Biosample. Cell lines were frequently checked in morphology under microscopy
408 and tested for mycoplasma contamination but were not authenticated. All cell lines were
409 cultured in DMEM medium with 10% fetal bovine serum (FBS) at 37°C in 5% CO_2 (v/v),
410 except for peritoneal macrophages that were maintained in RPMI 1640 medium,

411 **Intestinal Organoids**

412 Isolated small intestines were opened longitudinally, washed three times with cold PBS,
413 removed the villi by scraping, and incubated twice in cold PBS with 2 mM EDTA for 15 min
414 on ice. After removing the EDTA medium, the fractions were incubated in 50 mL cold PBS
415 with a fierce shake and passed through a 70-µm cell strainer (BD Bioscience) to remove the
416 residual villous material. Isolated crypts were centrifuged at 300 g for 5 min to separate the
417 crypts with single cells. The centrifuged fractions were suspended and cultured in Matrigel
418 with medium (Advanced DMEM/F12 supplemented with penicillin/streptomycin, 10 mM
419 HEPES, Glutamax, 13N2, 13B27 (all from Invitrogen), and 1mM N-acetylcysteine (Sigma)
420 containing growth factors 50 ng mL^{-1} EGF, 100 ng mL^{-1} noggin, 1mg mL^{-1} R-spondin). The
421 organoid formation was observed and analyzed every day after plating.

422

423 **METHOD DETAILS**

424 **Expression Plasmids, Viruses, Reagents, and Antibodies**

425 Expression plasmids encoding Flag-, Myc-, or HA-tagged wild-type or mutations of human
426 TBK1, IRF3, and the reporters of IFNβ_Luc and 5xISRE_Luc have been described previously
427 (Liu, Chen et al., 2017, Zhang, Meng et al., 2017b). Flag- or HA-tagged human AMPKα1,
428 AMPKα2, caAMPKα1 and AMPKα1 kinase domains were constructed using the pRK5
429 mammalian expression vector. Site-directed mutagenesis about TBK1 S511A/D/E and
430 AMPKα1 T172D were generated by PCR-based cloning performed by a kit from Stratagene.
431 All coding sequences were verified by DNA sequencing, and the detailed information for
432 construction was provided in the attached Supplementary Table 2 and upon requirement.

433 The pharmacological reagent, Compound C (Selleck), AICAR (Selleck), 991 (Selleck), A-

434 769662 (Selleck), ABT-737 (Selleck), qVD-OPH (Selleck), S63845 (Selleck), MK2206 (Selleck),
435 Doxycycline (Sangon Biotech), 2-DG (Sangon Biotech), cGAMP (Invivogen), poly(I:C)
436 (Invivogen), poly (dA:dT) (Invivogen), puromycin (Yeasen), G418 (Yeasen), Hydroxyurea (HU)
437 (Sigma), and Lonidamine (Selleck) were purchased and used according to manual
438 instructions. Aldometanib was generated by Dr. Sheng-Cai Lin (Xiamen University, Xiamen).
439 The monoclonal anti-TBK1 (3504S, 1:5,000 dilution), anti-pTBK1(S172) (5483S, 1:3,000
440 dilution), anti-IRF3 (4302S, 1:2,000 dilution), anti-pIRF3 (S396) (4947S, 1:5,000 dilution),
441 anti-AMPKα (5831S, 1:1,000 dilution), anti-pAMPKα (T172) (50081S, 1:1,000 dilution), anti-
442 pACC (S79) (3661S, 1:1,000 dilution), anti-ACC (3676S, 1:1,000 dilution), anti-Myc (2276S,
443 1:3,000 dilution), and anti-HA (3724S, 1:5,000 dilution) antibodies were purchased from Cell
444 Signaling Technology. The anti-pIRF3 (S386) (ab76493, 1:3,000 dilution), anti-STING
445 (ab181125, 1:100 dilution) were purchased from Abcam, and the anti-α-tubulin (T6199,
446 1:10,000 dilution), anti-β-actin (A5441, 1:10,000 dilution), anti-GAPDH (EPR16891, 1:3000),
447 anti-HA (H9658, 1:200 dilution), and anti-Flag (M2) (F3165, 1:5,000 dilution) were purchased
448 from Sigma. The anti-rabbit IgG and anti-mouse IgG antibodies were purchased from Santa
449 Cruz. The anti-pTBK1 (S511) was generated in collaboration with Abcam, targeting the
450 phospho-TBK1 S511.
451
452 **Plasmids Transfection and Virus Infection of Cultured Cells**
453 Lipofectamine 3000 (Invitrogen), Polyethyleneimine (PEI, Polysciences), or Lipofectamine
454 RNAiMAX (Invitrogen) transfection reagents were used for the transfection of plasmids,
455 poly(dA:dT), and poly(I:C). Digitonin (Sigma) was used to induce cGAMP.
456
457 **CRISPR/Cas9-mediated Generation of AMPKα1/α2$^{-/-}$ and TBK1 Knock-in Cells**
458 Guide RNA sequences targeting AMPKα1 and α2 mRNA sequence (hAMPKα1, 5'-
459 AAAGTTTGAGTGCTCAGAAG -3', 5'- GTGATGGAATATGTCTCAGG -3'; hAMPKα2, 5'-
460 TCAATTAACAGGCCATAAAG -3', 5'- GTTATTTAAGAAGATCCGAG -3'), TBK1 S511A/D knock-in
461 mRNA sequence (hTBK1, 5'- TATTTAGCTTTCCAGTTCTC -3', 5'- TTCTATTGTTCCCTGAGAAC -3')
462 were used to clone the genes into the vector pX330, which were transfected into DLD1 cells

463 by LipofectAmine 3000, together with the pCas9-2A-GFP plasmid, or with pCas9-2A-GFP and
464 pMD18 in the case of TBK1 S511A/D knock-in generation. 36 hours after transfection, cells
465 with green fluorescence were sorted with a Flow Cytometer (BD FACS Aria II) and
466 propagated. Immunoblotting with anti-AMPK(or the sequencing of the genomic PCR
467 products) identified clones. All gRNAs used in the experiments were also attached in
468 Supplementary Table 1.
469
470 **Luciferase Reporter Assay**
471 HEK293 cells were transfected with indicated reporters (100 ng) bearing an open read frame
472 (ORF) coding Firefly luciferase, along with the pRL-Luc with Renilla luciferase coding as the
473 internal control for transfection and other expression vectors specified in the results section.
474 In brief, after 24 hours post-transfection, cells were lysed by passive lysis buffer (Promega),
475 and luciferase assays were performed using a dual luciferase assay kit (Promega), quantified
476 with POLARstar Omega (BMG Labtech) and normalized to the internal Renilla luciferase
477 control.
478
479 **Quantitative RT-PCR Assay**
480 The DLD1 cells stimulated with Hydroxyurea (HU), Camptothecin (CPT), or Etoposide (ETO)
481 were lysed, and total RNA was extracted using an RNAeasy extraction kit (Axygen). cDNA
482 was generated by a one-step iScript cDNA synthesis kit (Vazyme), and quantitative real-time
483 PCR was performed using the EvaGreen Qpcr MasterMix (Abm) and CFX96 real-time PCR
484 system (Bio-Rad). Relative quantification was expressed as 2-ΔCt, where Ct is the difference
485 between the primary Ct value of triplicates of the sample and an endogenous L19 mRNA
486 control. The primer sequences used are listed in the following:
487 hIL-1α, 5'- AGTGCTGCTGAAGGAGATGCCTGA -3', 5'- CCCCTGCCAAGCACACCCAGTA -3';
488 hIL-1β, 5'- ATGATGGCTTATTACAGTGGCAA -3', 5'- GTCGGAGATTCGTAGCTGGA -3';
489 RPL19, 5'- ATGTATCACAGCCTGTACCTG -3', 5'- TTCTTGGTCTCTTCCTCCTTG -3';
490 All primers used in the qRT-PCR assay were also attached in Supplementary Table 1.
491

492 **Coimmunoprecipitations and Immunoblottings**

493 HEK293 transfected with specified plasmids encoding Myc-, Flag-, or HA-tagged AMPKα1,
494 AMPKα2, TBK1s, and IRF3s was lysed using the modified MLB lysis buffer (20 mM Tris-Cl,
495 200 mM NaCl, 10 mM NaF, 1 mM NaV_2O_4, 1% NP-40, 20 mM β-glycerophosphate, and
496 protease inhibitor, pH 7.5) (Xu et al., 2014). Cell lysates were then subjected to
497 immunoprecipitation using the antibodies of anti-Flag (Sigma, F3165-5MG, 1:200 dilution),
498 anti-Myc (CST, 2276S, 1:200 dilution), or anti-HA (Sigma, H9658, 1:200 dilution) for
499 transfected or induced proteins. After 3-4 washes with the MLB, adsorbed proteins were
500 resolved by SDS-PAGE (Bio-Rad) and immunoblotting with the indicated antibodies. Cell
501 lysates were also analyzed using SDS-PAGE and immunoblotting to control the protein
502 abundance.

503

504 ***In vitro* Kinase Assay**

505 HEK293 cells were transfected with plasmids encoding Flag-, Myc-, or HA-tagged TBK1s or
506 AMPKα and lysed by the modified MLB lysis buffer after 24 hours of transfection.
507 Immunoprecipitations were performed by using anti-Flag (Sigma, F3165-5MG, 1:200
508 dilution), anti-Myc (2276S, 1:200 dilution), or anti-HA (CST, 3724S, 1:200 dilution) antibodies.
509 With two washes by the MLB and two washes by the kinase assay buffer (200 μM ATP, 200
510 μM AMP, 20 mM Tris-HCl, 1 mM EGTA, 5 mM $MgCl_2$, 0.02% 2-mercapto-Ethanol, 0.03% Brij-
511 35, and 0.2 mg mL^{-1} BSA, PH 7.4), immunoprecipitated TBK1s and AMPKα1 were incubated
512 in the kinase assay buffer at 30°C for 60 min on THERMO-SHAKER (1400 rpm/min). The
513 reaction was stopped by adding 2 × SDS loading buffer and subjected to SDS-PAGE and
514 specified immunoblotting.

515

516 **Cellular senescence assays**

517 To evaluate damage-induced cellular senescence, cells at approximately 60-70% confluence
518 were treated with Hydroxyurea (HU, 10 mM), Camptothecin (CPT, 1 μM), Etoposide (ETO,
519 25 μM) or Mitomycin (MMC, 1 μM) for 24 hours, replaced with fresh medium, and cultured
520 for another 5 days and harvested for SA-β-Gal assay, by using a cellular senescence assay kit
521 (Yeasen 40754ES60) and according to the manufacturer's manual. Images were acquired

522 using a converted fluorescence microscope from Nikon. , cells were lysed after 5-8 days
523 stimulations and subjected to RNA extraction and qRT-PCR assays as described in the
524 previous section, to detect the senescence-associated secretory phenotype (SASPs), such as
525 the expression of cytokines including IL-1α and IL-1β.

526 **Senescence assays in zebrafish**

527 Zebrafish embryos were treated with 50 nM CPT with/without 1mM AICAR or 10 μM
528 Compound C from 1.5 days post fertilization (dpf) to 3.5 dpf and then fixed in 4%
529 paraformaldehyde in PBS at 4°C. After 3 washes with PBS (pH 7.4 and pH 6.0) at 4°C, SA-β-
530 Gal staining was performed according to the manual of the senescence assay kit (Yeasen
531 40754ES60). Animals were photographed under a dissecting microscope.

532

533 **Murine allograft growth of B16 melanoma**

534 C57BL/6 wild-type mice were maintained under specific-pathogen-free (SPF) conditions and
535 randomly selected for tumor injection. Six- to eight-week-old mice were administered a
536 subcutaneous injection of 1.5×10^6 B16-F10 melanoma cells and treated with or without
537 AICAR (5 mg/kg) or once a day, Aldometanib was supplied either through oral
538 gavaging(Zhang et al., 2022a). From the ninth-day post-tumor inoculation, the injected mice
539 were monitored for tumor growth daily as described in the protocols approved by the IACUC
540 of Zhejiang University. Other treatment regimens included: cGAMP, 2 μg intratumoral
541 injection every 3 days, starting on day 5 post-implantation; Lonidamine, 25 mg/kg
542 intraperitoneal injection every 3 days, starting on day 4 post-implantation. Tumor size is
543 presented as a square caliper measurement and was calculated based on two perpendicular
544 diameters (mm^2). The maximum diameter of tumors is limited up to 10 mm by ethical
545 permission, upon which the mice were sacrificed and considered as dead due to tumor
546 burden.

547

548 **Murine tumor Immunohistochemistry**

549 For immunohistochemistry assays, tumor samples were dissected, fixed in 4%
550 paraformaldehyde for 12 hours at 4°C, dehydrated with 30% sucrose overnight at 4°C,

embedded in optimal cutting temperature compound, and immediately frozen at -80°C. The sectioned samples at 10 µm thickness were washed two times with PBS, permeabilized with 0.5% Triton X-100, blocked in 3% horse serum in PBS for 30 min, and incubated sequentially with primary antibodies, including anti-CD3 (Abcam, 16669, 1:100 dilution), anti-CD4 (eBioscience, 14976680, 1:100 dilution), anti-CD8 (eBioscience, 14080880, 1:100 dilution), and anti-F4/80 (Bio-Rad, MCA497RT, 1:100 dilution). After the sections were incubated with Alexa-labeled secondary antibodies (Jackson, 111-095-003, 1:500 dilutions, Invitrogen, A11006, 1:1000 dilutions) and extensively washed, they were stained with DAPI (Santa Cruz Biotech) and mounted with ProLong™ Gold antifade reagent (Invitrogen). Immunofluorescence images were obtained and analyzed using a Zeiss LSM710 or LSM 880 confocal microscope.

Nano-liquid Chromatography/Tandem MS (Nano LC-MS/MS) Analysis

Phoenix National Proteomics Core services performed Nano LC/tandem MS analysis for protein identification and characterization and label-free quantification. Tryptic peptides were separated on a C18 column and analyzed by LTQ-Orbitrap Velos (Thermo). Proteins were identified using the National Center for Biotechnology Information search engine against the human or mouse RefSeq protein databases. The mass spectrometry proteomics data of TBK1 modifications by AMPK have been deposited to the ProteomeXchange Consortium (http://proteomecentral.proteomexchange.org) via the iProX partner repository with the dataset identifier PXD033926.

QUANTIFICATION AND STATISTICAL ANALYSIS

Quantitative data are presented as the mean ± standard error of the mean (SEM) from at least three independent experiments. When appropriate, the statistically significant differences between multiple comparisons were analyzed using the one-way or two-way ANOVA test with Bonferroni correction. Differences were considered significant at $p<0.05$. All samples were included in the analyses if preserved and properly processed, and no samples or animals were excluded except for zebrafish with conventional injection damage.

No statistical method was used to predetermine sample size, and all experiments except those involving animals were not randomized. Immunoblotting, reporter assays, and qRT-PCR experiments have been repeated a minimum of three times independently to ensure reproducibility. The investigators were not blinded to allocation during experiments and outcome assessment.

REFERENCES

Ablasser A, Goldeck M, Cavlar T, Deimling T, Witte G, Rohl I, Hopfner KP, Ludwig J, Hornung V (2013) cGAS produces a 2'-5'-linked cyclic dinucleotide second messenger that activates STING. *Nature* 498: 380-4

Bakhoum SF, Ngo B, Laughney AM, Cavallo JA, Murphy CJ, Ly P, Shah P, Sriram RK, Watkins TBK, Taunk NK, Duran M, Pauli C, Shaw C, Chadalavada K, Rajasekhar VK, Genovese G, Venkatesan S, Birkbak NJ, McGranahan N, Lundquist M et al. (2018) Chromosomal instability drives metastasis through a cytosolic DNA response. *Nature* 553: 467-472

Cerboni S, Jeremiah N, Gentili M, Gehrmann U, Conrad C, Stolzenberg MC, Picard C, Neven B, Fischer A, Amigorena S, Rieux-Laucat F, Manel N (2017) Intrinsic antiproliferative activity of the innate sensor STING in T lymphocytes. *J Exp Med* 214: 1769-1785

Chan YK, Gack MU (2015) RIG-I-like receptor regulation in virus infection and immunity. *Curr Opin Virol* 12: 7-14

Chen C, Xu P (2023) Cellular functions of cGAS-STING signaling. *Trends Cell Biol* 33: 630-648

Chen Q, Boire A, Jin X, Valiente M, Er EE, Lopez-Soto A, Jacob L, Patwa R, Shah H, Xu K, Cross JR, Massague J (2016a) Carcinoma-astrocyte gap junctions promote brain metastasis by cGAMP transfer. *Nature* 533: 493-498

Chen Q, Sun L, Chen ZJ (2016b) Regulation and function of the cGAS-STING pathway of cytosolic DNA sensing. *Nat Immunol* 17: 1142-9

Chen S, Liu S, Wang J, Wu Q, Wang A, Guan H, Zhang Q, Zhang D, Wang X, Song H, Qin J, Zou J, Jiang Z, Ouyang S, Feng XH, Liang T, Xu P (2020) TBK1-Mediated DRP1 Targeting Confers Nucleic Acid Sensing to Reprogram Mitochondrial Dynamics and Physiology. *Mol Cell* 80: 810-827 e7

Chiappinelli KB, Strissel PL, Desrichard A, Li H, Henke C, Akman B, Hein A, Rote NS, Cope LM, Snyder A, Makarov V, Budhu S, Slamon DJ, Wolchok JD, Pardoll DM, Beckmann MW, Zahnow CA, Merghoub T, Chan TA, Baylin SB et al. (2015) Inhibiting DNA Methylation Causes an Interferon Response in Cancer via dsRNA Including Endogenous Retroviruses. *Cell* 162: 974-86

Chin EN, Sulpizio A, Lairson LL (2022) Targeting STING to promote antitumor immunity. *Trends Cell Biol*

Clements VK, Long T, Long R, Figley C, Smith DMC, Ostrand-Rosenberg S (2018) Frontline Science: High fat diet and leptin promote tumor progression by inducing myeloid-derived suppressor cells. *J Leukoc Biol* 103: 395-407

Concepcion AR, Wagner LE, 2nd, Zhu J, Tao AY, Yang J, Khodadadi-Jamayran A, Wang YH, Liu M, Rose RE, Jones DR, Coetzee WA, Yule DI, Feske S (2022) The volume-regulated anion channel LRRC8C suppresses T cell function by regulating cyclic dinucleotide transport and STING-p53 signaling. *Nat Immunol* 23: 287-302

Corton JM, Gillespie JG, Hawley SA, Hardie DG (1995) 5-aminoimidazole-4-carboxamide ribonucleoside. A specific method for activating AMP-activated protein kinase in intact cells? *Eur J Biochem* 229: 558-65

Dou Z, Ghosh K, Vizioli MG, Zhu J, Sen P, Wangensteen KJ, Simithy J, Lan Y, Lin Y, Zhou Z, Capell BC, Xu C, Xu M, Kieckhaefer JE, Jiang T, Shoshkes-Carmel M, Tanim K, Barber GN, Seykora JT, Millar SE et al. (2017) Cytoplasmic chromatin triggers inflammation in senescence and cancer. *Nature* 550: 402-406

Fitzgerald KA, McWhirter SM, Faia KL, Rowe DC, Latz E, Golenbock DT, Coyle AJ, Liao SM, Maniatis T (2003) IKKepsilon and TBK1 are essential components of the IRF3 signaling pathway. *Nat Immunol* 4: 491-6

Floridi A, Paggi MG, Marcante ML, Silvestrini B, Caputo A, De Martino C (1981) Lonidamine, a selective inhibitor of aerobic glycolysis of murine tumor cells. *J Natl Cancer Inst* 66: 497-9

Gao P, Ascano M, Wu Y, Barchet W, Gaffney BL, Zillinger T, Serganov AA, Liu Y, Jones RA, Hartmann G, Tuschl T, Patel DJ (2013) Cyclic [G(2',5')pA(3',5')p] is the metazoan second messenger produced by DNA-activated cyclic GMP-AMP synthase. *Cell* 153: 1094-107

Garcia D, Shaw RJ (2017) AMPK: Mechanisms of Cellular Energy Sensing and Restoration of Metabolic Balance.

Mol Cell 66: 789-800

Ghosh M, Saha S, Bettke J, Nagar R, Parrales A, Iwakuma T, van der Velden AWM, Martinez LA (2021) Mutant p53 suppresses innate immune signaling to promote tumorigenesis. *Cancer Cell* 39: 494-508 e5

Gluck S, Guey B, Gulen MF, Wolter K, Kang TW, Schmacke NA, Bridgeman A, Rehwinkel J, Zender L, Ablasser A (2017) Innate immune sensing of cytosolic chromatin fragments through cGAS promotes senescence. *Nat Cell Biol* 19: 1061-1070

Gonzalez A, Hall MN, Lin SC, Hardie DG (2020) AMPK and TOR: The Yin and Yang of Cellular Nutrient Sensing and Growth Control. *Cell Metab* 31: 472-492

Gui X, Yang H, Li T, Tan X, Shi P, Li M, Du F, Chen ZJ (2019) Autophagy induction via STING trafficking is a primordial function of the cGAS pathway. *Nature* 567: 262-266

Gulen MF, Koch U, Haag SM, Schuler F, Apetoh L, Villunger A, Radtke F, Ablasser A (2017) Signalling strength determines proapoptotic functions of STING. *Nat Commun* 8: 427

Hardie DG, Ashford ML (2014) AMPK: regulating energy balance at the cellular and whole body levels. *Physiology (Bethesda)* 29: 99-107

Hardie DG, Ross FA, Hawley SA (2012) AMPK: a nutrient and energy sensor that maintains energy homeostasis. *Nat Rev Mol Cell Biol* 13: 251-62

Hong C, Schubert M, Tijhuis AE, Requesens M, Roorda M, van den Brink A, Ruiz LA, Bakker PL, van der Sluis T, Pieters W, Chen M, Wardenaar R, van der Vegt B, Spierings DCJ, de Bruyn M, van Vugt M, Foijer F (2022) cGAS-STING drives the IL-6-dependent survival of chromosomally instable cancers. *Nature* 607: 366-373

Hu MM, Shu HB (2020) Innate Immune Response to Cytoplasmic DNA: Mechanisms and Diseases. *Annu Rev Immunol* 38: 79-98

Incio J, Liu H, Suboj P, Chin SM, Chen IX, Pinter M, Ng MR, Nia HT, Grahovac J, Kao S, Babykutty S, Huang Y, Jung K, Rahbari NN, Han X, Chauhan VP, Martin JD, Kahn J, Huang P, Desphande V et al. (2016) Obesity-Induced Inflammation and Desmoplasia Promote Pancreatic Cancer Progression and Resistance to Chemotherapy. *Cancer Discov* 6: 852-69

Ishikawa H, Barber GN (2008) STING is an endoplasmic reticulum adaptor that facilitates innate immune signalling. *Nature* 455: 674-8

Keerthana CK, Rayginia TP, Shifana SC, Anto NP, Kalimuthu K, Isakov N, Anto RJ (2023) The role of AMPK in cancer metabolism and its impact on the immunomodulation of the tumor microenvironment. *Front Immunol* 14: 1114582

Klil-Drori AJ, Azoulay L, Pollak MN (2017) Cancer, obesity, diabetes, and antidiabetic drugs: is the fog clearing? *Nat Rev Clin Oncol* 14: 85-99

Kwon J, Bakhoum SF (2020) The Cytosolic DNA-Sensing cGAS-STING Pathway in Cancer. *Cancer Discov* 10: 26-39

Li S, Mirlekar B, Johnson BM, Brickey WJ, Wrobel JA, Yang N, Song D, Entwistle S, Tan X, Deng M, Cui Y, Li W, Vincent BG, Gale M, Jr., Pylayeva-Gupta Y, Ting JP (2022) STING-induced regulatory B cells compromise NK function in cancer immunity. *Nature* 610: 373-380

Lin SC, Hardie DG (2018) AMPK: Sensing Glucose as well as Cellular Energy Status. *Cell Metab* 27: 299-313

Liu S, Cai X, Wu J, Cong Q, Chen X, Li T, Du F, Ren J, Wu YT, Grishin NV, Chen ZJ (2015) Phosphorylation of innate immune adaptor proteins MAVS, STING, and TRIF induces IRF3 activation. *Science* 347: aaa2630

Liu S, Chen S, Li X, Wu S, Zhang Q, Jin Q, Hu L, Zhou R, Yu Z, Meng F, Wang S, Huang Y, Ye S, Shen L, Xia Z, Zou J, Feng XH, Xu P (2017) Lck/Hck/Fgr-Mediated Tyrosine Phosphorylation Negatively Regulates TBK1 to Restrain Innate Antiviral Responses. *Cell Host Microbe* 21: 754-768 e5

Mackenzie KJ, Carroll P, Martin CA, Murina O, Fluteau A, Simpson DJ, Olova N, Sutcliffe H, Rainger JK, Leitch A, Osborn RT, Wheeler AP, Nowotny M, Gilbert N, Chandra T, Reijns MAM, Jackson AP (2017) cGAS surveillance

of micronuclei links genome instability to innate immunity. *Nature* 548: 461-465

McArthur K, Whitehead LW, Heddleston JM, Li L, Padman BS, Oorschot V, Geoghegan ND, Chappaz S, Davidson S, San Chin H, Lane RM, Dramicanin M, Saunders TL, Sugiana C, Lessene R, Osellame LD, Chew TL, Dewson G, Lazarou M, Ramm G et al. (2018) BAK/BAX macropores facilitate mitochondrial herniation and mtDNA efflux during apoptosis. *Science* 359

Melki I, Rose Y, Uggenti C, Van Eyck L, Fremond ML, Kitabayashi N, Rice GI, Jenkinson EM, Boulai A, Jeremiah N, Gattorno M, Volpi S, Sacco O, Terheggen-Lagro SWJ, Tiddens H, Meyts I, Morren MA, De Haes P, Wouters C, Legius E et al. (2017) Disease-associated mutations identify a novel region in human STING necessary for the control of type I interferon signaling. *J Allergy Clin Immunol* 140: 543-552 e5

Meng F, Yu Z, Zhang D, Chen S, Guan H, Zhou R, Wu Q, Zhang Q, Liu S, Venkat Ramani MK, Yang B, Ba XQ, Zhang J, Huang J, Bai X, Qin J, Feng XH, Ouyang S, Zhang YJ, Liang T et al. (2021) Induced phase separation of mutant NF2 imprisons the cGAS-STING machinery to abrogate antitumor immunity. *Mol Cell* 81: 4147-4164 e7

Mouchiroud L, Eichner LJ, Shaw RJ, Auwerx J (2014) Transcriptional coregulators: fine-tuning metabolism. *Cell Metab* 20: 26-40

Petrasek J, Iracheta-Vellve A, Csak T, Satishchandran A, Kodys K, Kurt-Jones EA, Fitzgerald KA, Szabo G (2013) STING-IRF3 pathway links endoplasmic reticulum stress with hepatocyte apoptosis in early alcoholic liver disease. *Proc Natl Acad Sci U S A* 110: 16544-9

Pilli M, Arko-Mensah J, Ponpuak M, Roberts E, Master S, Mandell MA, Dupont N, Ornatowski W, Jiang S, Bradfute SB, Bruun JA, Hansen TE, Johansen T, Deretic V (2012) TBK-1 promotes autophagy-mediated antimicrobial defense by controlling autophagosome maturation. *Immunity* 37: 223-34

Ramakrishnan G, Terry AR, Nogueira V, Magdy A, Hay N (2025) Deletion of AMP-activated protein kinase impairs metastasis and is rescued by ROS scavenging or ectopic CD36 expression. *Cell Rep* 44: 115183

Reinfeld BI, Madden MZ, Wolf MM, Chytil A, Bader JE, Patterson AR, Sugiura A, Cohen AS, Ali A, Do BT, Muir A, Lewis CA, Hongo RA, Young KL, Brown RE, Todd VM, Huffstater T, Abraham A, O'Neil RT, Wilson MH et al. (2021) Cell-programmed nutrient partitioning in the tumour microenvironment. *Nature* 593: 282-288

Roberts DJ, Tan-Sah VP, Ding EY, Smith JM, Miyamoto S (2014) Hexokinase-II positively regulates glucose starvation-induced autophagy through TORC1 inhibition. *Mol Cell* 53: 521-33

Rodrigues Mantuano N, Stanczak MA, Oliveira IA, Kirchhammer N, Filardy AA, Monaco G, Santos RC, Fonseca AC, Fontes M, Bastos CS, Jr., Dias WB, Zippelius A, Todeschini AR, Laubli H (2020) Hyperglycemia Enhances Cancer Immune Evasion by Inducing Alternative Macrophage Polarization through Increased O-GlcNAcylation. *Cancer Immunol Res* 8: 1262-1272

Roers A, Hiller B, Hornung V (2016) Recognition of Endogenous Nucleic Acids by the Innate Immune System. *Immunity* 44: 739-54

Rongvaux A, Jackson R, Harman CC, Li T, West AP, de Zoete MR, Wu Y, Yordy B, Lakhani SA, Kuan CY, Taniguchi T, Shadel GS, Chen ZJ, Iwasaki A, Flavell RA (2014) Apoptotic caspases prevent the induction of type I interferons by mitochondrial DNA. *Cell* 159: 1563-77

Samson N, Ablasser A (2022) The cGAS-STING pathway and cancer. *Nat Cancer* 3: 1452-1463

Sasaki N, Homme M, Murayama T, Osaki T, Tenma T, An T, Takegami Y, Tani T, Gedeon PC, Kobayashi Y, Canadas I, Barbie DA, Yao R, Kitajima S (2024) RNA sensing induced by chromosome missegregation augments antitumor immunity. *Mol Cell*

Sharma S, tenOever BR, Grandvaux N, Zhou GP, Lin R, Hiscott J (2003) Triggering the interferon antiviral response through an IKK-related pathway. *Science* 300: 1148-51

Sun L, Wu J, Du F, Chen X, Chen ZJ (2013) Cyclic GMP-AMP synthase is a cytosolic DNA sensor that activates the

719 type I interferon pathway. *Science* 339: 786-91
720 Sun W, Li Y, Chen L, Chen H, You F, Zhou X, Zhou Y, Zhai Z, Chen D, Jiang Z (2009) ERIS, an endoplasmic reticulum
721 IFN stimulator, activates innate immune signaling through dimerization. *Proc Natl Acad Sci U S A* 106: 8653-8
722 Takeuchi O, Akira S (2010) Pattern recognition receptors and inflammation. *Cell* 140: 805-20
723 White MJ, McArthur K, Metcalf D, Lane RM, Cambier JC, Herold MJ, van Delft MF, Bedoui S, Lessene G, Ritchie
724 ME, Huang DC, Kile BT (2014) Apoptotic caspases suppress mtDNA-induced STING-mediated type I IFN
725 production. *Cell* 159: 1549-62
726 Wild P, Farhan H, McEwan DG, Wagner S, Rogov VV, Brady NR, Richter B, Korac J, Waidmann O, Choudhary C,
727 Dotsch V, Bumann D, Dikic I (2011) Phosphorylation of the autophagy receptor optineurin restricts
728 Salmonella growth. *Science* 333: 228-33
729 Wu J, Sun L, Chen X, Du F, Shi H, Chen C, Chen ZJ (2013) Cyclic GMP-AMP is an endogenous second messenger
730 in innate immune signaling by cytosolic DNA. *Science* 339: 826-30
731 Wu S, Zhang Q, Zhang F, Meng F, Liu S, Zhou R, Wu Q, Li X, Shen L, Huang J, Qin J, Ouyang S, Xia Z, Song H, Feng
732 XH, Zou J, Xu P (2019) HER2 recruits AKT1 to disrupt STING signalling and suppress antiviral defence and
733 antitumour immunity. *Nat Cell Biol* 21: 1027-1040
734 Wu YQ, Zhang CS, Xiong J, Cai DQ, Wang CZ, Wang Y, Liu YH, Wang Y, Li Y, Wu J, Wu J, Lan B, Wang X, Chen S,
735 Cao X, Wei X, Hu HH, Guo H, Yu Y, Ghafoor A et al. (2023) Low glucose metabolite 3-phosphoglycerate
736 switches PHGDH from serine synthesis to p53 activation to control cell fate. *Cell Res* 33: 835-850
737 Xu P, Bailey-Bucktrout S, Xi Y, Xu D, Du D, Zhang Q, Xiang W, Liu J, Melton A, Sheppard D, Chapman HA,
738 Bluestone JA, Derynck R (2014) Innate antiviral host defense attenuates TGF-beta function through IRF3-
739 mediated suppression of Smad signaling. *Mol Cell* 56: 723-37
740 Yang H, Wang H, Ren J, Chen Q, Chen ZJ (2017) cGAS is essential for cellular senescence. *Proc Natl Acad Sci U S*
741 *A* 114: E4612-E4620
742 Zhang C, Shang G, Gui X, Zhang X, Bai XC, Chen ZJ (2019) Structural basis of STING binding with and
743 phosphorylation by TBK1. *Nature* 567: 394-398
744 Zhang CS, Hawley SA, Zong Y, Li M, Wang Z, Gray A, Ma T, Cui J, Feng JW, Zhu M, Wu YQ, Li TY, Ye Z, Lin SY, Yin H,
745 Piao HL, Hardie DG, Lin SC (2017a) Fructose-1,6-bisphosphate and aldolase mediate glucose sensing by
746 AMPK. *Nature* 548: 112-116
747 Zhang CS, Jiang B, Li M, Zhu M, Peng Y, Zhang YL, Wu YQ, Li TY, Liang Y, Lu Z, Lian G, Liu Q, Guo H, Yin Z, Ye Z,
748 Han J, Wu JW, Yin H, Lin SY, Lin SC (2014) The lysosomal v-ATPase-Ragulator complex is a common activator
749 for AMPK and mTORC1, acting as a switch between catabolism and anabolism. *Cell Metab* 20: 526-40
750 Zhang CS, Li M, Wang Y, Li X, Zong Y, Long S, Zhang M, Feng JW, Wei X, Liu YH, Zhang B, Wu J, Zhang C, Lian W,
751 Ma T, Tian X, Qu Q, Yu Y, Xiong J, Liu DT et al. (2022a) The aldolase inhibitor aldometanib mimics glucose
752 starvation to activate lysosomal AMPK. *Nat Metab* 4: 1369-1401
753 Zhang D, Liu Y, Zhu Y, Zhang Q, Guan H, Liu S, Chen S, Mei C, Chen C, Liao Z, Xi Y, Ouyang S, Feng XH, Liang T,
754 Shen L, Xu P (2022b) A non-canonical cGAS-STING-PERK pathway facilitates the translational program critical
755 for senescence and organ fibrosis. *Nat Cell Biol* 24: 766-782
756 Zhang Q, Liu S, Zhang CS, Wu Q, Yu X, Zhou R, Meng F, Wang A, Zhang F, Chen S, Wang X, Li L, Huang J, Huang
757 YW, Zou J, Qin J, Liang T, Feng XH, Lin SC, Xu P (2022c) AMPK directly phosphorylates TBK1 to integrate
758 glucose sensing into innate immunity. *Mol Cell* 82: 4519-4536 e7
759 Zhang Q, Meng F, Chen S, Plouffe SW, Wu S, Liu S, Li X, Zhou R, Wang J, Zhao B, Liu J, Qin J, Zou J, Feng XH, Guan
760 KL, Xu P (2017b) Hippo signalling governs cytosolic nucleic acid sensing through YAP/TAZ-mediated TBK1
761 blockade. *Nat Cell Biol* 19: 362-374
762 Zhang X, Shi H, Wu J, Zhang X, Sun L, Chen C, Chen ZJ (2013) Cyclic GMP-AMP containing mixed phosphodiester

linkages is an endogenous high-affinity ligand for STING. *Mol Cell* 51: 226-35

Zhao P, Wong KI, Sun X, Reilly SM, Uhm M, Liao Z, Skorobogatko Y, Saltiel AR (2018) TBK1 at the Crossroads of Inflammation and Energy Homeostasis in Adipose Tissue. *Cell* 172: 731-743 e12

Zhong B, Yang Y, Li S, Wang YY, Li Y, Diao F, Lei C, He X, Zhang L, Tien P, Shu HB (2008) The adaptor protein MITA links virus-sensing receptors to IRF3 transcription factor activation. *Immunity* 29: 538-50

Zhou R, Wang M, Li X, Liu Y, Yao Y, Wang A, Chen C, Zhang Q, Wu Q, Zhang Q, Neculai D, Xia B, Shao JZ, Feng XH, Liang T, Zou J, Wang X, Xu P (2024) TBK1-Zyxin signaling controls tumor-associated macrophage recruitment to mitigate antitumor immunity. *EMBO J* 43: 4984-5017

773 **FIGURE LEGENDS**

774 **Figure 1. Glucose deficiency promotes intratumoral cGAS-STING signaling. (A-B)**, The
775 intratumoral glucose deficiency state in B16-F10 melanoma was validated through
776 immunofluorescence of phospho-ACC1 (pACC), a primary substrate of AMPK, by which an
777 evident signal of pACC was seen in the edge of melanoma (A). AMPK agonist AICAR
778 treatment was set as the positive control (B). Scale bars=50 μm**. (C-E),** Cytosolic dsDNA
779 sensing was evaluated in PMs (C), MEFs (D), and DLD1 (E) under 2-DG or AICAR (AMPK
780 agonist) administration in response to STING agonist cGAMP, as indicated by
781 immunoblotting using antibodies recognizing active forms of TBK1 and IRF3. **(F-G)**, Sensing
782 of mtDNAs, released upon the treatment of ABT-737, qVD-OPH, and S63845 (AQS), was
783 similarly augmented by glucose depletion, revealed by the phosphorylation level of TBK1.
784 **(H)**, The effects of AICAR administration on TpdAdT-induced DNA sensing were evaluated in
785 DLD1, representing enhanced dsDNA sensing to double-stranded DNA. ***Applied to figures 1-***
786 ***6***: unless specified, n=3 independent experiments (mean±SEM); *, P<0.05, **, P<0.01, and
787 ***, P<0.001, by statistical analysis of the indicated comparison with ANOVA and Bonferroni
788 correction.

789

790 **Figure 2. AMPK facilitates cGAS-STING signaling in cancer cells by TBK1 S511**
791 **phosphorylation. (A)**, Double knockout (dKO) of AMPK α1 and α2 impaired the activation of
792 TBK1 and IRF3 following DMXAA stimulation in B16-F10 melanoma cells. **(B)**, The genetic
793 ablation of AMPK α1 and α2 subunits reduced TpIC-induced cytosolic RNA sensing in HCT116,
794 revealed by a significant decrease in phosphorylation of TBK1 and IRF3. **(C)**,
795 Coimmunoprecipitation assay revealed coexpression of AMPKα1 or caAMPKα1 (activated
796 AMPKα1) enhanced this association of TBK1 and IRF3 2SA. **(D)**, Reporter assay showed that
797 the expression of AMPK α1 and α2 subunits strongly promoted TBK1-stimulated IRF3
798 transactivation with IFNβ promoter in HEK293 cells. **(E)**, Mass spectrometry analysis
799 identified that AMPKα1 phosphorylated the S511 residue of TBK1, and the phosphorylation
800 was completely inhibited by the AMPK inhibitor dorsomorphin (Compound C). **(F)**,
801 caAMPKα1 and AMPKa1 kinase domain directly phosphorylated TBK1 at S511 in vitro kinase
802 assay. **(G-H)**, TBK1 mutants S511A (resistant to AMPK modification) exhibited significantly

803 reduced activity IRF3-responsive reporter assays (G) and a weaker interaction with IRF3 2SA
804 (H). Meanwhile, TBK1 S511E (mimics AMPK-phosphorylated TBK1) demonstrated a strong
805 potential to bind and activate IRF3. **(I-J)**, Generated DLD1 knock-in (KI) clones with mutations
806 that either prevent (S511A) or mimic (S511D) AMPK-mediated modification using CRISPR-
807 based genome editing. cGAMP-stimulated cGAS-STING pathway was weakened in TBK1
808 S511A KI cells (I) but strengthened in S511D KI cells (J).
809
810 **Figure 3. AMPK drives STING-induced senescence and apoptosis of cancer cells and**
811 **organoids.** **(A-B)**, Chemical induction of DNA damage in DLD1 gut epithelial cells by CPT,
812 mitomycin C (MMC), etoposide (ETO), and hydroxyurea (HU) treatment led to a robust
813 phenotype of cellular senescence, as assessed by SA-β-Gal staining (A) and SASP features,
814 including the mRNA expression of IL1α and IL1β (B). Genetic ablation of AMPKα1/α2 in
815 DLD1 cells prevented DNA sensing-initiated cellular senescence (A). Conversely, AICAR
816 treatment significantly enhanced DNA damage-induced cellular senescence (B). Scale bars =
817 100 µm. **(C)**, Energy deficiency stimulation of AMPK by 2-DG or AICAR led to an exaggerated
818 phenotype of cellular senescence in DLD1 cells, particularly upon HU-induced DNA damage.
819 Scale bars = 100 µm. ***, P<0.001, by ANOVA with Bonferroni correction. **(D)**, Cellular
820 senescence was assessed in zebrafish embryos (n=30) subjected to chemical-induced
821 damage by incubation with CPT (50 nM) and to SA-β-Gal staining. A strong phenotype of
822 cellular senescence was detected in the heads and tails of zebrafish; this phenotype was
823 mildly upregulated by AICAR treatment but was mitigated by dorsomorphin. Scale bars = 500
824 µm. **(E)**, FACS analyses of early and late apoptotic cells among DLD1 cells revealed that
825 activation of AMPK by AICAR promoted cell apoptosis induced by cytosolic DNA sensing,
826 which triggered by DNA damage inducer HU, but inhibition of AMPK by dorsomorphin
827 suppressed HU-induced apoptosis. **(F)**, Intestinal crypts were isolated from mice at 6 weeks
828 of age and cultured *in vitro* in the absence or presence of the AMPK agonist AICAR. PI
829 staining revealed that cytosolic DNA sensing stimulated by the DNA damage inducer HU
830 resulted in robust apoptosis of intestinal cells in organoids, and AICAR exaggerated this
831 effect. Scale bars=50 µm. n=15 intestinal organoids examined (mean±SEM). *, P=0.002,
832 compared with wild-type organoids (ANOVA with Bonferroni correction).

833

834 **Figure 4. AMPK-TBK1 signaling facilitates STING-mediated antitumor immunity in**
835 **melanomas.** **(A-C)**, The STING SAVI mutant (R281Q) was constitutively active (caSTING). The
836 volumes (A), weights (B), and photos (C) of the subcutaneously B16-F10 melanoma growth
837 in wild-type C57BL/6 mice revealed a markedly decreased growth in melanomas expressing
838 the STING SAVI mutant (R281Q). AICAR administration further increased this effect of STING
839 signaling, resulting in robust tumor growth arrest. n=12 inoculations per group (mean ±
840 SEM), measured 7 days post tumor inoculation (dpti). **(D-E)**, The administration of AICAR
841 with caSTING profoundly increased immune cell infiltration, particularly the infiltration of
842 the $CD4^+$ and $CD8^+$ T cells into melanomas, as detected by Immunohistochemistry (IHC)
843 upon STING SAVI mutant expression (D). The statistics for the immunohistochemistry-
844 positive cells were calculated (E). Scale bars=20 µm. **, P<0.01, and ***, P<0.001, by ANOVA
845 with Bonferroni correction. **(F-H)**, B16-F10 melanoma cells were implanted subcutaneously
846 into $TBK1^{WT/WT}$ or $TBK1^{S511E/S511E}$ C57BL/6 mice with intratumoral injection of cGAMP.
847 Volumes (F), weights (G), and photos (H) of melanoma revealed that melanoma growth was
848 markedly attenuated in these $TBK1^{S511E/S511E}$ mice. **(I-J)**, Immunohistochemistry (I), and
849 statistics (J) showed B16-F10 melanoma from $TBK1^{S511E/S511E}$ mice accompanied with the
850 increased immune cell infiltration. Stimulation in $TBK1^{S511E/S511E}$ mice by cGAMP did not
851 further enhance the infiltrated T cells and antitumor immunity effect. Scale bars=20 µm.

852

853 **Figure 5. AMPK agonists synergize well with cGAMP to promote antitumor immunity in**
854 **melanomas.** **(A-C)**, The weights (A), volumes (B), and photos (C) of the subcutaneously B16-
855 F10 melanoma growth in wild-type C57BL/6 mice with administration of cGAMP or AICAR.
856 AICAR administration further promoted the antitumor immunity effect of cGAMP-induced
857 STING signaling, inhibiting tumor growth. n=6 inoculations per group (mean ± SEM). **(D-F)**,
858 The weights (D), volumes (E), and photos (F) of the subcutaneously B16-F10 melanoma
859 growth in wild-type C57BL/6 mice with administration of Aldometanib and cGAMP. Adding
860 AICAR enhanced the suppression of tumor growth induced by cGAMP. n=4 inoculations per
861 group (mean ± SEM). **(G-I)**, Administration of Aldometanib alone inhibited the growth of
862 AMPK dKO B16-F10 tumors in WT mice. The weights (G), volumes (H), and photos (I) showed

863 similar tumor sizes of AMPK dKO B16-F10 tumors with the treatment of Aldometanib or
864 cGAMP. n=8 inoculations per group (mean ± SEM).
865
866 **Figure 6. Disrupting aerobic glycolysis potentiates antitumor immunity through the AMPK-**
867 **TBK1 cascade. (A-C)**, The administration of Lonidamine (Hexokinase inhibitor) with cGAMP
868 profoundly inhibited the growth of B16-F10 melanoma, revealed by the weights (A), volume
869 curve (B), and images (C) of B16-F10 melanoma. n=8 or 10 inoculations per group (mean ±
870 SEM). **(D-E)**, Enhanced infiltration of $CD3^+$, $CD4^{+,}$ and $CD8^+$ T lymphocytes were imaged in
871 B16-F10 melanomas with the administration of Lonidamine and cGAMP; Scale bars, 20 µm.
872 (H) n=3 per group (mean ± SEM). **(I)**, Immunohistochemistry showed that Lonidamine
873 treatment enhanced cGAMP-induced cGAS-STING signaling in B16-F10 melanomas, as
874 evidenced by increased levels of phosphorylated STING (pSTING S365) and phosphorylated
875 TBK1 (pTBK1 S172), and total intratumoral STING protein levels; Scale bars=20 µm.

Figure 1

A

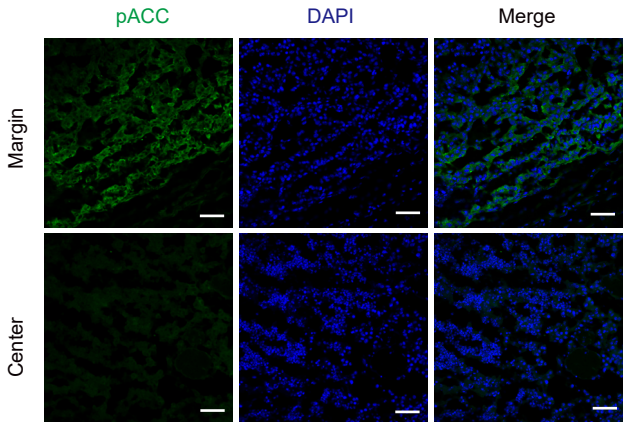

B16-F10 Tumor/DMSO

B

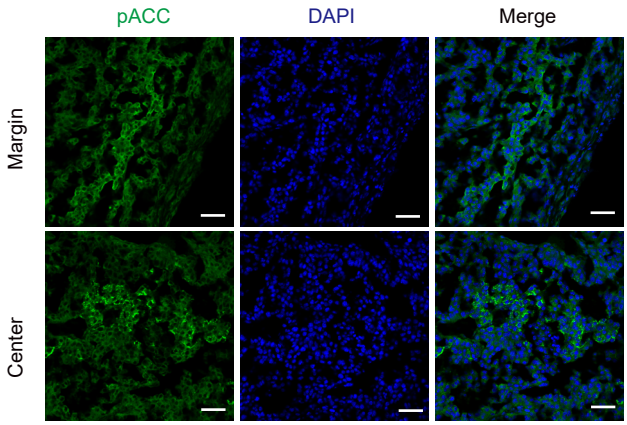

B16-F10 Tumor/AICAR

C

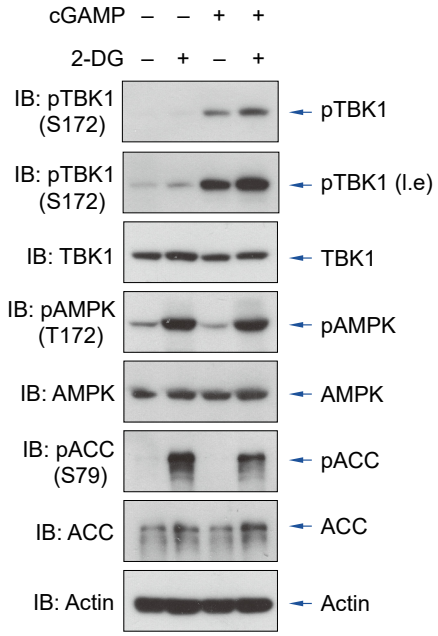

PMs

D

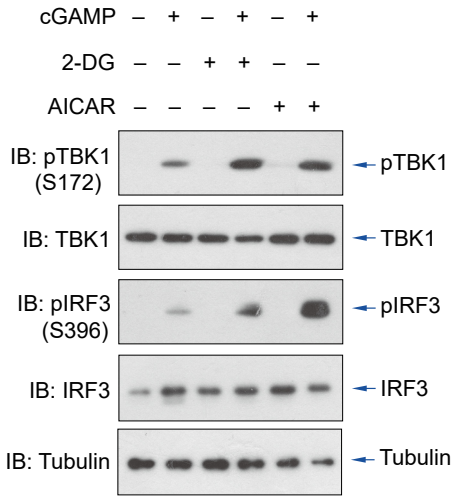

MEFs

E

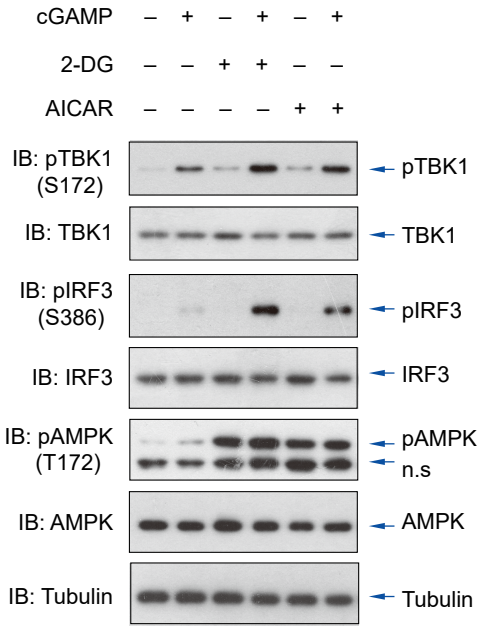

DLD1

F

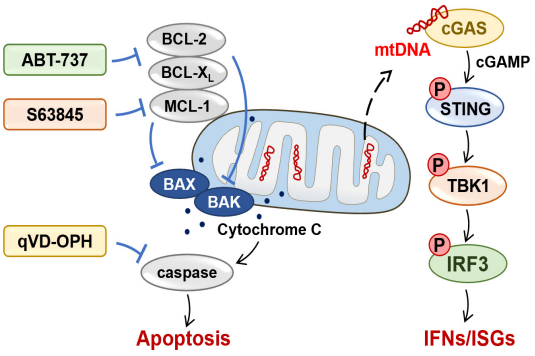

G

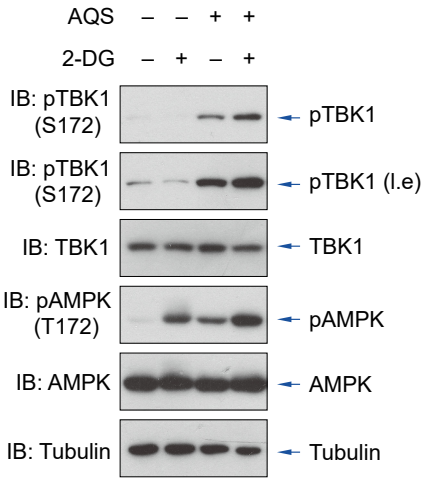

DLD1

H

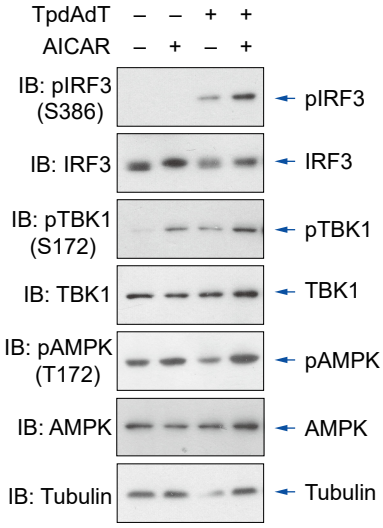

DLD1

Figure 2

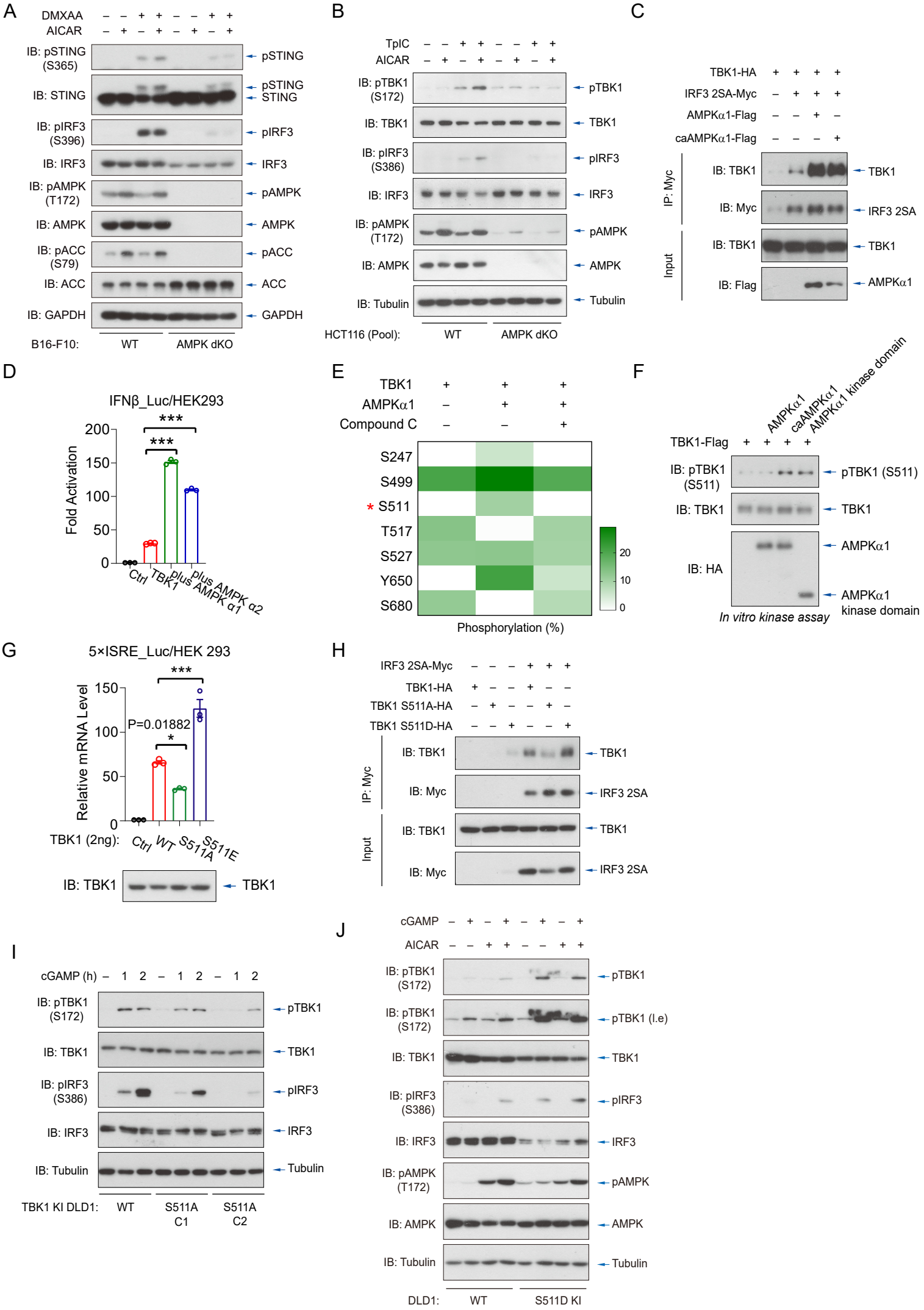
A
DMXAA
AICAR
IB: pSTING (S365)
IB: STING
IB: pIRF3 (S396)
IB: IRF3
IB: pAMPK (T172)
IB: AMPK
IB: pACC (S79)
IB: ACC
IB: GAPDH
pSTING
STING
pIRF3
IRF3
pAMPK
AMPK
pACC
ACC
GAPDH
B16-F10:
WT
AMPK dKO
B
TpIC
AICAR
IB: pTBK1 (S172)
IB: TBK1
IB: pIRF3 (S386)
IB: IRF3
IB: pAMPK (T172)
IB: AMPK
IB: Tubulin
pTBK1
TBK1
pIRF3
IRF3
pAMPK
AMPK
Tubulin
HCT116 (Pool):
WT
AMPK dKO
C
TBK1-HA
IRF3 2SA-Myc
AMPKα1-Flag
caAMPKα1-Flag
IP: Myc
Input
IB: TBK1
IB: Myc
IB: TBK1
IB: Flag
TBK1
IRF3 2SA
TBK1
AMPKα1
D
IFNβ_Luc/HEK293
Fold Activation
200
150
100
50
0
***
***
Ctrl
TBK1
plus AMPK α1
plus AMPK α2
E
TBK1
AMPKα1
Compound C
S247
S499
* S511
T517
S527
Y650
S680
20
10
0
Phosphorylation (%)
F
AMPKα1
caAMPKα1
AMPKα1 kinase domain
TBK1-Flag
IB: pTBK1 (S511)
IB: TBK1
IB: HA
pTBK1 (S511)
TBK1
AMPKα1
AMPKα1 kinase domain
In vitro kinase assay
G
5×ISRE_Luc/HEK 293
Relative mRNA Level
150
100
50
0
***
P=0.01882
*
TBK1 (2ng):
Ctrl
WT
S511A
S511E
IB: TBK1
TBK1
H
IRF3 2SA-Myc
TBK1-HA
TBK1 S511A-HA
TBK1 S511D-HA
IP: Myc
Input
IB: TBK1
IB: Myc
IB: TBK1
IB: Myc
TBK1
IRF3 2SA
TBK1
IRF3 2SA
I
cGAMP (h)
IB: pTBK1 (S172)
IB: TBK1
IB: pIRF3 (S386)
IB: IRF3
IB: Tubulin
pTBK1
TBK1
pIRF3
IRF3
Tubulin
TBK1 KI DLD1:
WT
S511A C1
S511A C2
J
cGAMP
AICAR
IB: pTBK1 (S172)
IB: pTBK1 (S172)
IB: TBK1
IB: pIRF3 (S386)
IB: IRF3
IB: pAMPK (T172)
IB: AMPK
IB: Tubulin
pTBK1
pTBK1 (l.e)
TBK1
pIRF3
IRF3
pAMPK
AMPK
Tubulin
DLD1:
WT
S511D KI

Figure 3

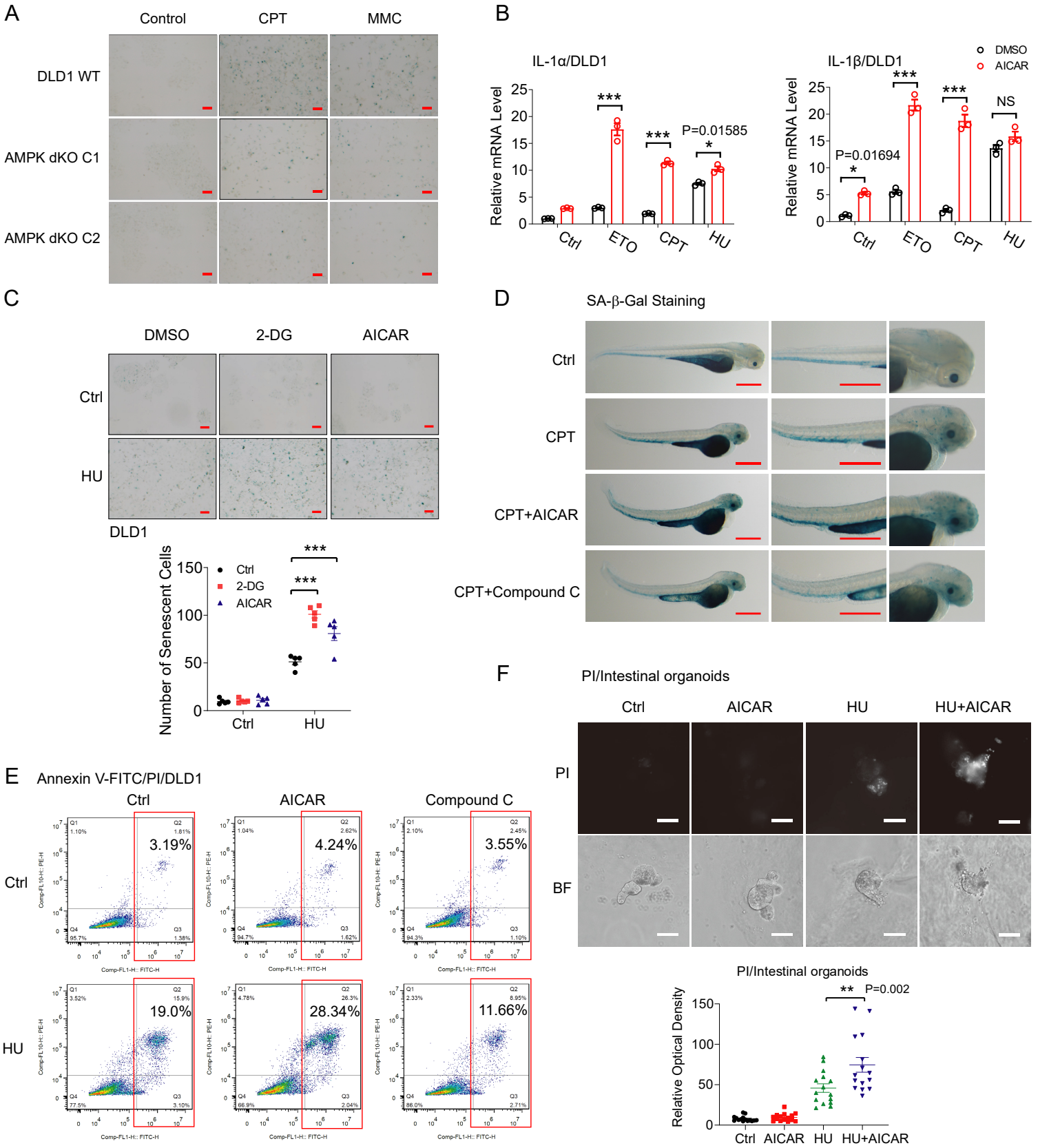
A
Control
CPT
MMC
DLD1 WT
AMPK dKO C1
AMPK dKO C2
B
IL-1α/DLD1
Relative mRNA Level
***
***
P=0.01585
*
Ctrl
ETO
CPT
HU
IL-1β/DLD1
DMSO
AICAR
P=0.01694
NS
C
DMSO
2-DG
AICAR
Ctrl
HU
DLD1
Number of Senescent Cells
Ctrl
2-DG
AICAR
D
SA-β-Gal Staining
Ctrl
CPT
CPT+AICAR
CPT+Compound C
E
Annexin V-FITC/PI/DLD1
Ctrl
AICAR
Compound C
3.19%
4.24%
3.55%
19.0%
28.34%
11.66%
F
PI/Intestinal organoids
Ctrl
AICAR
HU
HU+AICAR
PI
BF
PI/Intestinal organoids
Relative Optical Density
**
P=0.002

Figure 4

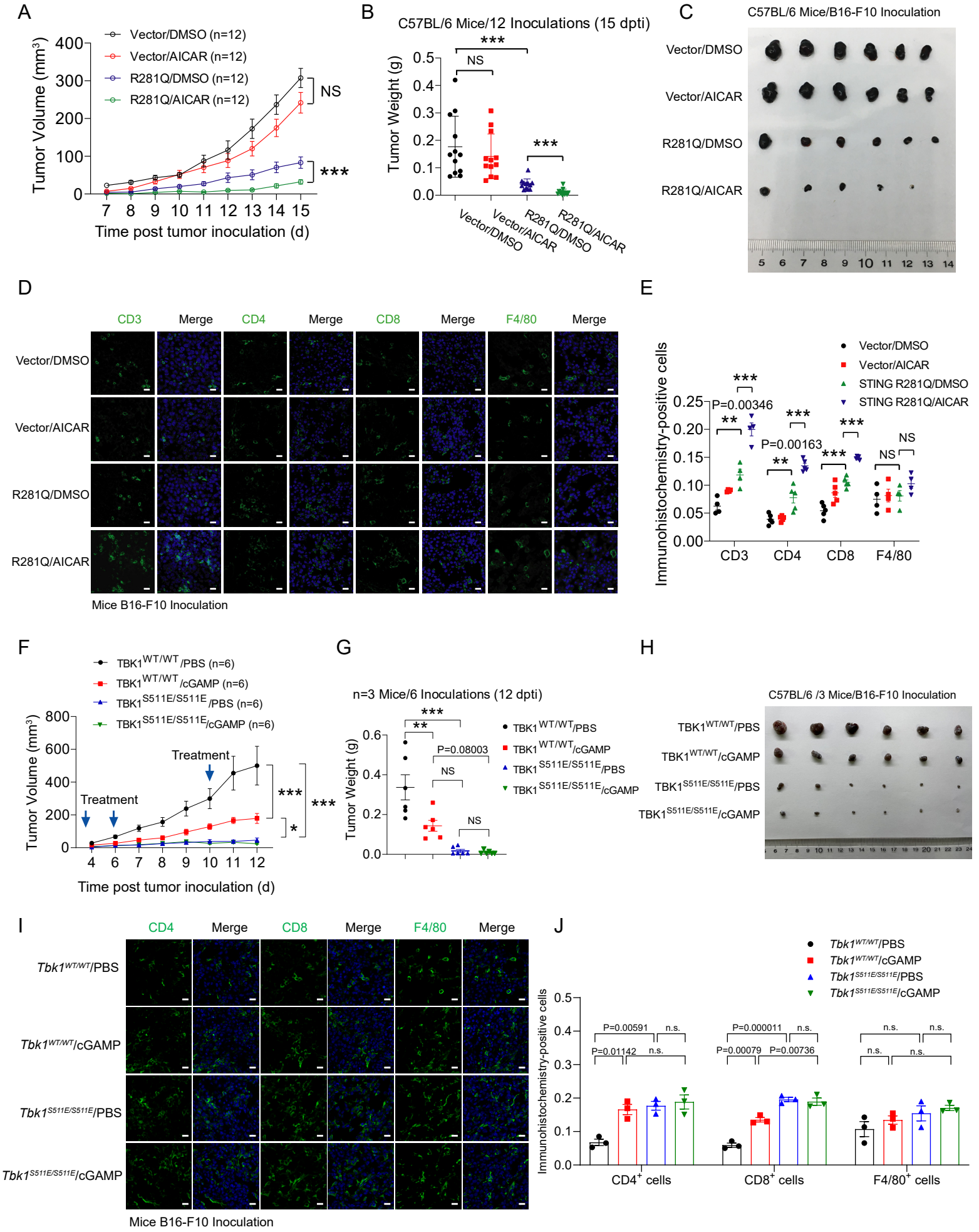
A
Vector/DMSO (n=12)
Vector/AICAR (n=12)
R281Q/DMSO (n=12)
R281Q/AICAR (n=12)
Tumor Volume (mm³)
Time post tumor inoculation (d)
NS
***
B
C57BL/6 Mice/12 Inoculations (15 dpti)
Tumor Weight (g)
Vector/DMSO
Vector/AICAR
R281Q/DMSO
R281Q/AICAR
C
C57BL/6 Mice/B16-F10 Inoculation
D
CD3
Merge
CD4
CD8
F4/80
Mice B16-F10 Inoculation
E
Immunohistochemistry-positive cells
STING R281Q/DMSO
STING R281Q/AICAR
P=0.00346
P=0.00163
F
TBK1WT/WT/PBS (n=6)
TBK1WT/WT/cGAMP (n=6)
TBK1S511E/S511E/PBS (n=6)
TBK1S511E/S511E/cGAMP (n=6)
Treatment
G
n=3 Mice/6 Inoculations (12 dpti)
P=0.08003
H
C57BL/6 /3 Mice/B16-F10 Inoculation
I
Tbk1WT/WT/PBS
Tbk1WT/WT/cGAMP
Tbk1S511E/S511E/PBS
Tbk1S511E/S511E/cGAMP
J
P=0.00591
P=0.01142
P=0.000011
P=0.00079
P=0.00736
n.s.
CD4+ cells
CD8+ cells
F4/80+ cells

Figure 5

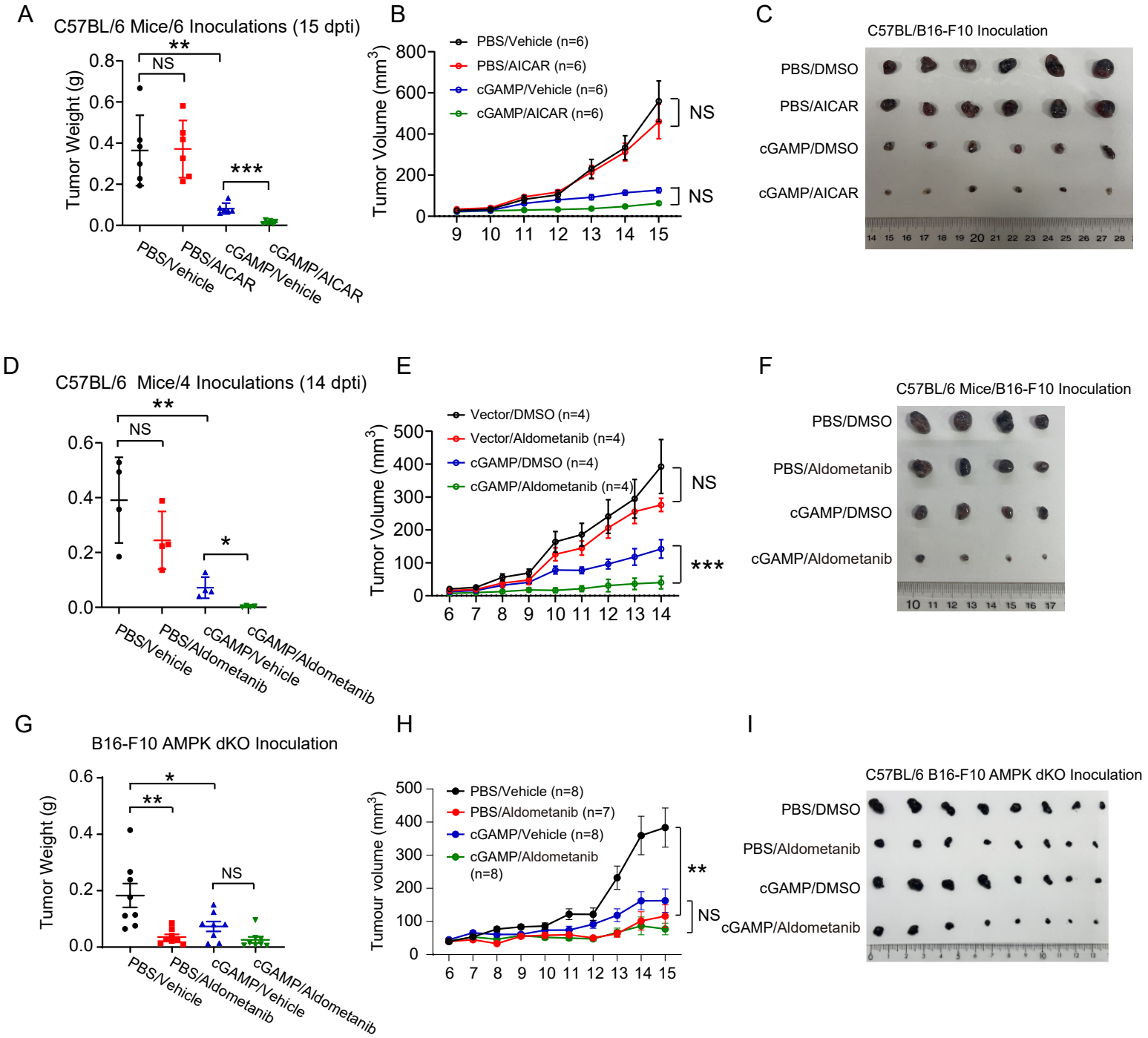
A
C57BL/6 Mice/6 Inoculations (15 dpti)
Tumor Weight (g)
0.8
0.6
0.4
0.2
0.0
**
NS
***
PBS/Vehicle
PBS/AICAR
cGAMP/Vehicle
cGAMP/AICAR
B
Tumor Volume (mm3)
800
600
400
200
0
PBS/Vehicle (n=6)
PBS/AICAR (n=6)
cGAMP/Vehicle (n=6)
cGAMP/AICAR (n=6)
NS
NS
9 10 11 12 13 14 15
C
C57BL/B16-F10 Inoculation
PBS/DMSO
PBS/AICAR
cGAMP/DMSO
cGAMP/AICAR
D
C57BL/6 Mice/4 Inoculations (14 dpti)
0.6
0.4
0.2
0.0
**
NS
*
PBS/Vehicle
PBS/Aldometanib
cGAMP/Vehicle
cGAMP/Aldometanib
E
Tumor Volume (mm3)
500
400
300
200
100
0
Vector/DMSO (n=4)
Vector/Aldometanib (n=4)
cGAMP/DMSO (n=4)
cGAMP/Aldometanib (n=4)
NS
***
6 7 8 9 10 11 12 13 14
F
C57BL/6 Mice/B16-F10 Inoculation
PBS/DMSO
PBS/Aldometanib
cGAMP/DMSO
cGAMP/Aldometanib
G
B16-F10 AMPK dKO Inoculation
Tumor Weight (g)
0.6
0.4
0.2
0.0
*
**
NS
PBS/Vehicle
PBS/Aldometanib
cGAMP/Vehicle
cGAMP/Aldometanib
H
Tumour volume (mm3)
500
400
300
200
100
0
PBS/Vehicle (n=8)
PBS/Aldometanib (n=7)
cGAMP/Vehicle (n=8)
cGAMP/Aldometanib (n=8)
**
NS
6 7 8 9 10 11 12 13 14 15
I
C57BL/6 B16-F10 AMPK dKO Inoculation
PBS/DMSO
PBS/Aldometanib
cGAMP/DMSO
cGAMP/Aldometanib

Figure 6

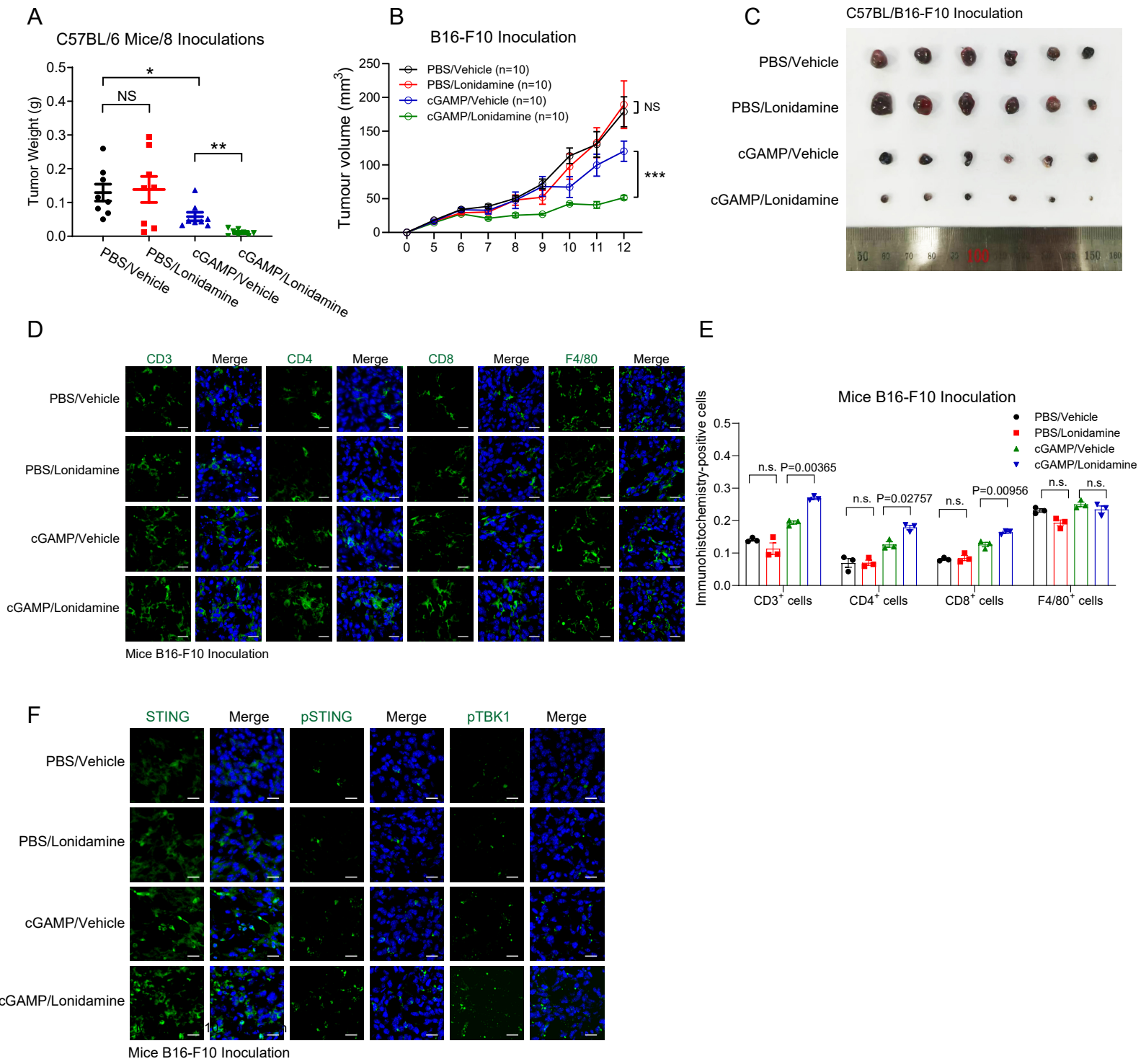
A
C57BL/6 Mice/8 Inoculations
Tumor Weight (g)
0.5
0.4
0.3
0.2
0.1
0.0
*
NS
**
PBS/Vehicle
PBS/Lonidamine
cGAMP/Vehicle
cGAMP/Lonidamine
B
B16-F10 Inoculation
Tumour volume (mm3)
250
200
150
100
50
0
PBS/Vehicle (n=10)
PBS/Lonidamine (n=10)
cGAMP/Vehicle (n=10)
cGAMP/Lonidamine (n=10)
NS
***
0 5 6 7 8 9 10 11 12
C
C57BL/B16-F10 Inoculation
PBS/Vehicle
PBS/Lonidamine
cGAMP/Vehicle
cGAMP/Lonidamine
D
CD3
Merge
CD4
Merge
CD8
Merge
F4/80
Merge
PBS/Vehicle
PBS/Lonidamine
cGAMP/Vehicle
cGAMP/Lonidamine
Mice B16-F10 Inoculation
E
Mice B16-F10 Inoculation
Immunohistochemistry-positive cells
0.5
0.4
0.3
0.2
0.1
0.0
PBS/Vehicle
PBS/Lonidamine
cGAMP/Vehicle
cGAMP/Lonidamine
n.s.
P=0.00365
n.s.
P=0.02757
n.s.
P=0.00956
n.s.
n.s.
CD3+ cells
CD4+ cells
CD8+ cells
F4/80+ cells
F
STING
Merge
pSTING
Merge
pTBK1
Merge
PBS/Vehicle
PBS/Lonidamine
cGAMP/Vehicle
cGAMP/Lonidamine
Mice B16-F10 Inoculation

Figure 1

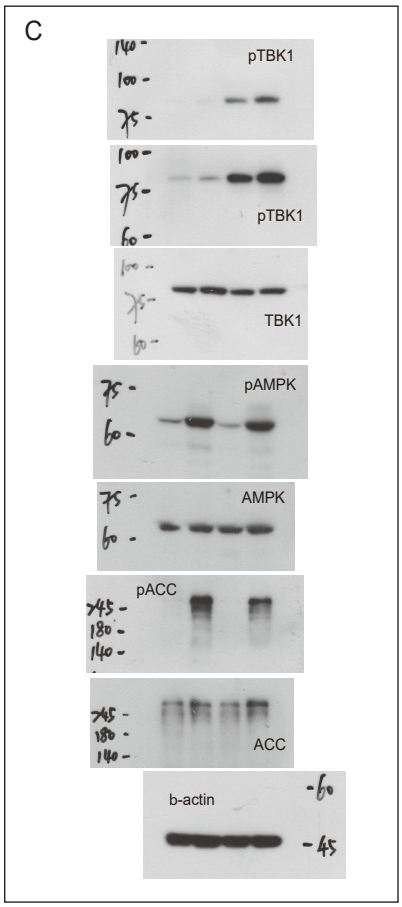

Figure 1

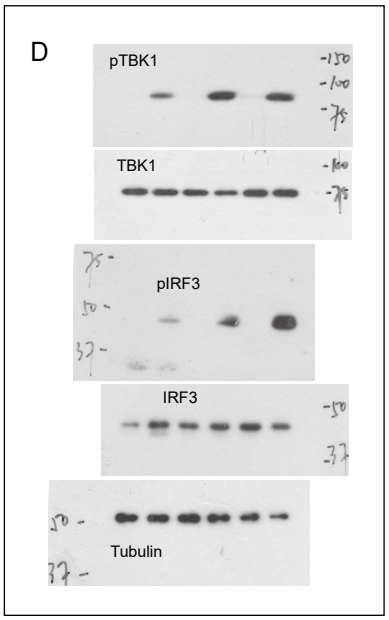

Figure 1

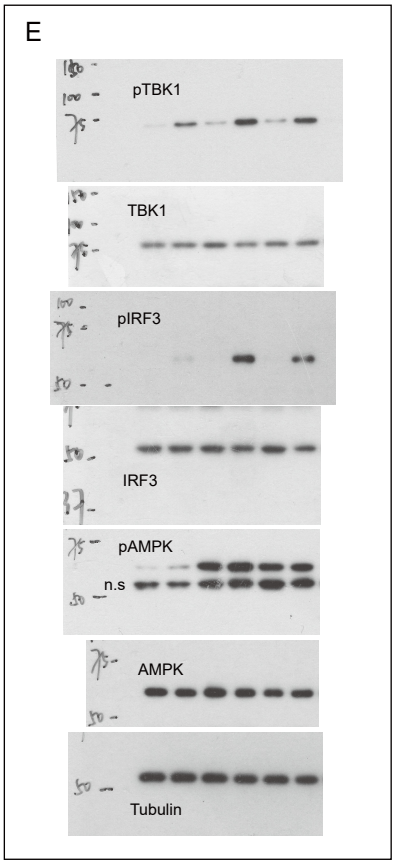

Figure 1

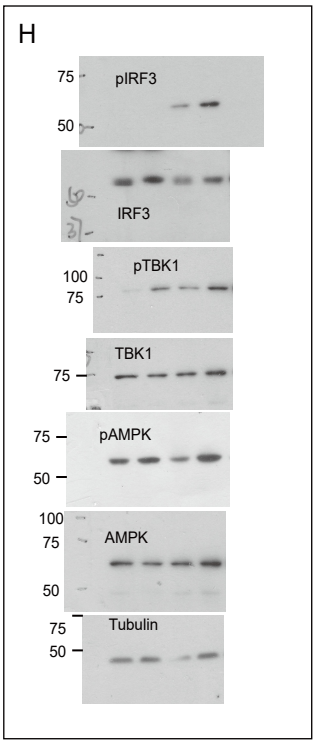

Figure 1

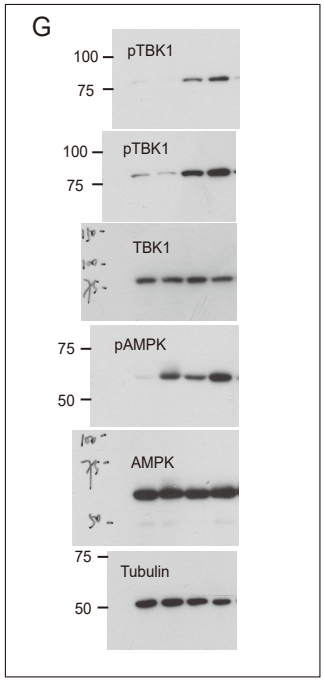

Figure 2

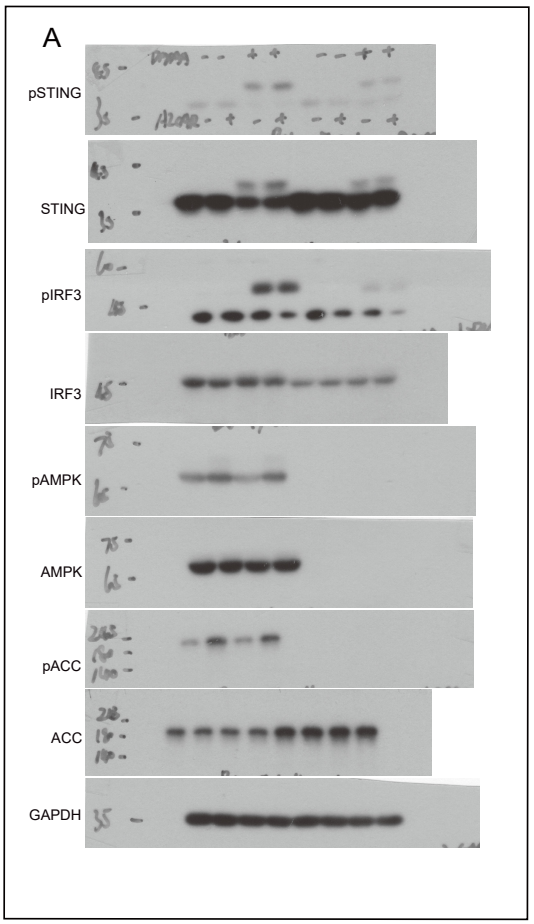

Figure 2

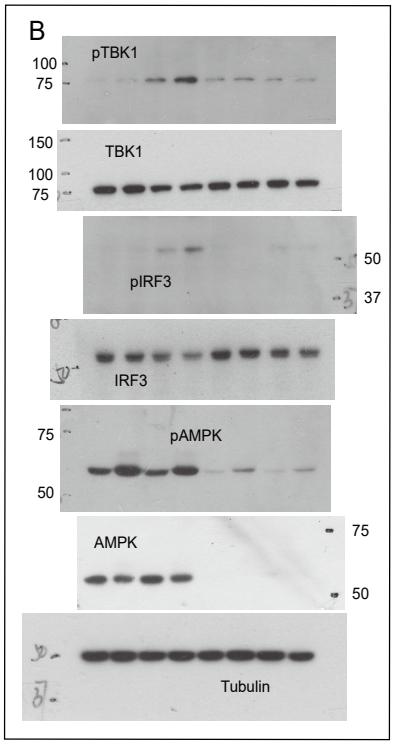

Figure 2

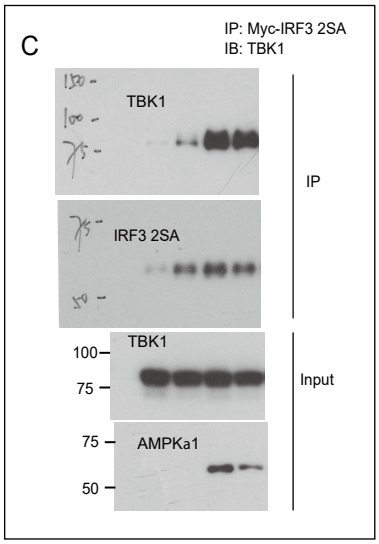

Figure 2

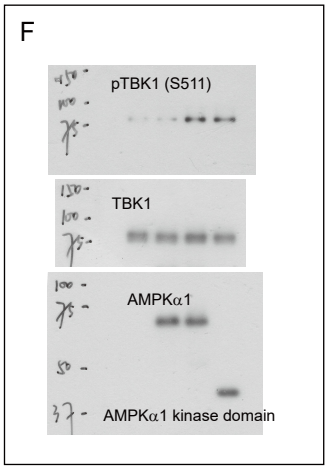

Figure 2

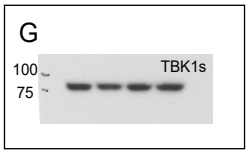

Figure 2

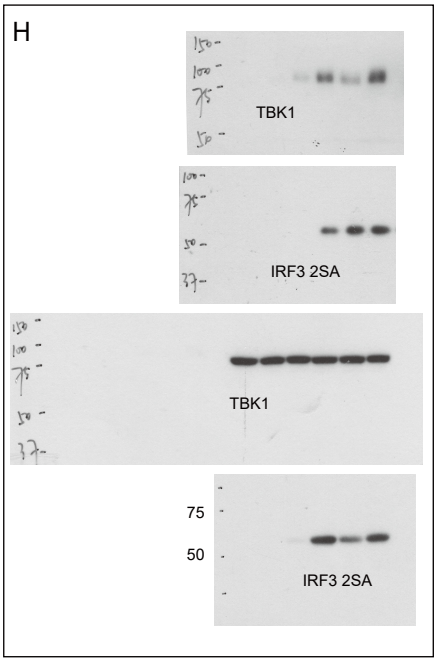

Figure 2

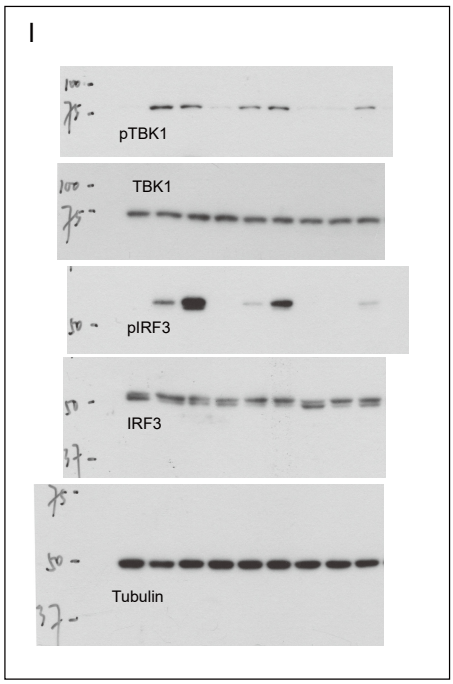

Figure 2

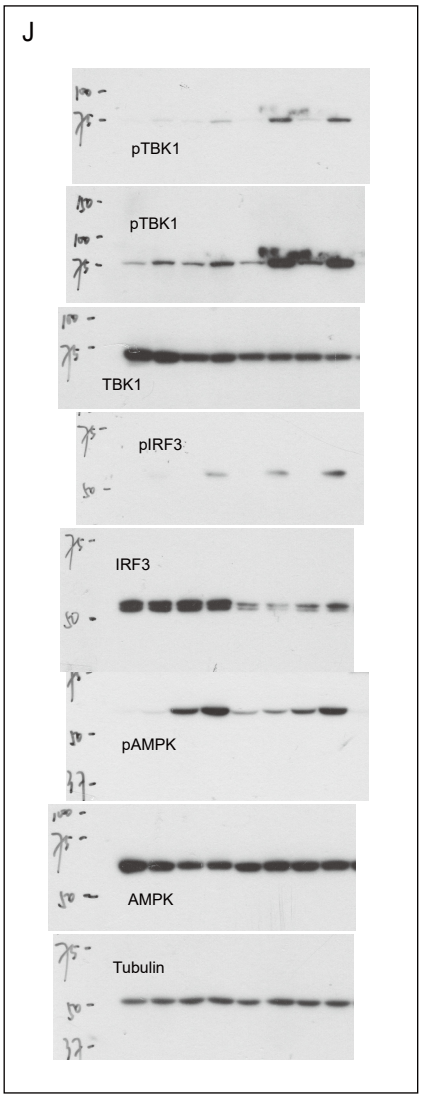

Suppl. Table 1_Oligos Used in Study

qPCR Primers	Sequence	Species	Company
IL-1a-Forward Primer	5' - AGTGCTGCTGAAGGAGATGCCTGA - 3'	human	biosune
IL-1a-Reverse Primer	5' - CCCCTGCCAAGCACACCCAGTA - 3'	human	biosune
IL-1b-Forward Primer	5' - ATGATGGCTTATTACAGTGGCAA - 3'	human	biosune
IL-1b-Reverse Primer	5' - GTCGGAGATTCGTAGCTGGA - 3'	human	biosune
RPL19-Forward Primer	5' - ATGTATCACAGCCTGTACCTG - 3'	human	biosune
RPL19-Reverse Primer	5' - TTCTTGGTCTCTTCCTCCTTG - 3'	human	biosune

Primers

Cas9 Primers	Sequence	Species	Company
AMPKα1-Cas9-Forward Primer	5' - CACCGAAAGTTTGAGTGCTCAGAAG - 3'	human	biosune
AMPKα1-Cas9-Reverse Primer	5' - AAACCTTCTGAGCACTCAAACTTTC - 3'	human	biosune
AMPKα2-Cas9-Forward Primer	5' - CACCGTCAATTAACAGGCCATAAAG - 3'	human	biosune
AMPKα2-Cas9-Reverse Primer	5' - AAACCTTTATGGCCTGTTAATTGAC - 3'	human	biosune
TBK1-S511A/D-Knock-In-Forward Primer	5' - CACCGTATTTAGCTTTCCAGTTCTC - 3'	human	biosune
TBK1-S511A/D-Knock-In-Reverse Primer	5' - AAACGAGAACTGGAAAGCTAAATAC - 3'	human	biosune

Suppl. Table 2_ List of Recombinant DNA

DNA	SOURCE	IDENTIFIER
pRK5-HA-TBK1 S511A	This paper	N/A
pRK5-HA-TBK1 S511D	This paper	N/A
pRK5-HA-TBK1 S511E	This paper	N/A
pRK5-Flag-TBK1 S511A	This paper	N/A
pRK5-Flag-TBK1 S511D	This paper	N/A
pRK5-Flag-TBK1 S511E	This paper	N/A
pRK5-HA-AMPKα1	This paper	N/A
pRK5-HA-AMPKα1 T172D	This paper	N/A
pRK5-HA-AMPKα1 kinase domain (1-312)	This paper	N/A
pRK5-Flag-AMPKα1	This paper	N/A
pRK5-Flag-TBK1	Lab stored	N/A
pRK5-HA-TBK1	Lab stored	N/A
pRK5-Myc-TBK1	Lab stored	N/A
pRK5-Myc-IRF3	Lab stored	N/A
pRK5-Myc-IRF3 2SA	Lab stored	N/A
pIFNβ_Luc	Lab stored	N/A
p5xISRE_Luc	Lab stored	N/A
gRNA	Lab stored	N/A
Cas9-2A-GFP	Lab stored	N/A
pMD18	Lab stored	N/A
pX330	Addgene	Cat#42230

Suppl. Table 3_Statistics Source Data
(See details in the following sheets)